MIT Open Access Articles

Revisiting the Schrage Equation for Kinetically Limited Evaporation and Condensation

Massachusetts Institute of Technology

Revisiting the Schrage Equation for Kinetically Limited Evaporation and Condensation

Geoffrey Vaartstra
Department of Mechanical Engineering,
Massachusetts Institute of Technology,
Cambridge, MA 02139

Zhengmao Lu
Department of Materials Science and
Engineering,
Massachusetts Institute of Technology,
Cambridge, MA 02139

John H. Lienhard
Department of Mechanical Engineering,
Massachusetts Institute of Technology,
Cambridge, MA 02139

Evelyn N. Wang[1]
Department of Mechanical Engineering,
Massachusetts Institute of Technology,
Cambridge, MA 02139
e-mail: enwang@mit.edu

The Schrage equation is commonly used in thermofluid engineering to model high-rate liquid–vapor phase change of pure fluids. Although shortcomings of this simple model were pointed out decades ago and more rigorous models have emerged from the kinetic theory community, Schrage's equation continues to be widely used. In this paper, we quantify the accuracy of the Schrage equation for evaporation and condensation of monatomic and polyatomic fluids at the low to moderately high flux operating conditions relevant to thermofluid engineering applications. As a high-accuracy reference, we numerically solve a Bhatnagar, Gross, and Krook (BGK)-like a model equation for polyatomic vapors that have previously been shown to produce accurate solutions to the Boltzmann transport equation. We observe that the Schrage equation overpredicts heat/mass fluxes by ∼15% for fluids with accommodation coefficients close to unity. For fluids with smaller accommodation coefficients, such as water, the Schrage equation yields more accurate flux estimates. We find that the Mott-Smith-like moment methods developed for liquid–vapor phase change are much more accurate than the Schrage equation, achieving heat/mass flux estimates that deviate by less than 1% (evaporation) and 4% (condensation) from the reference solution. In light of these results, we recommend using the moment method equations instead of the Schrage equation. We also provide tables with our high-accuracy numerical data for evaporation of any fluid and condensation of saturated water vapor, engineering equations fit our data, and code for moment method calculations of evaporation and condensation. [DOI: 10.1115/1.4054382]

Keywords: Schrage equation, evaporation, condensation, accommodation coefficient, kinetic theory, Knudsen layer, moment method, Hertz–Knudsen equation, evaporation coefficient, condensation coefficient, Boltzmann transport equation, liquid-vapor phase change, polyatomic vapor

1 Introduction

The Schrage equation is widely used by engineers to estimate heat/mass transfer rates of evaporation and condensation in the kinetically limited regime. This high-rate regime is defined by the dominance of the kinetic resistance at the liquid–vapor interface, which can occur when diffusional mass transfer resistances are absent. For example, the diffusion of vapor through the air is rate-limiting, but this resistance can be minimized in a hermetically sealed device. Thus, the Schrage equation holds great importance for modeling and design of systems that operate at high rates of evaporation/condensation, as found in applications such as power generation, refrigeration, electronics cooling, and distillation.

Schrage published his dissertation in 1953 [1], formulating what we refer to as the "Schrage equation" to correct the description of the half-space problem of evaporation and condensation previously discussed by Hertz [2] and Knudsen [3]. Specifically, Schrage accounted for the nonzero macroscopic velocity of the vapor phase resulting from the net evaporation/condensation flux. A similar treatment was given by Kucherov and Rikenglas [4], but here we focus on Schrage's formula. In 1991, Barrett and Clement [5] noted that Schrage's formulation violates the conservation of momentum and energy between the liquid–vapor interface and the far-field vapor. In fact, the seldom-mentioned fifth chapter of Schrage's thesis acknowledges this failure and seeks to rectify the issue of conservation. Schrage developed a solution based on conservation of mass, momentum, and energy very

similar to the "moment solutions" later applied by Anisimov [6] and Ytrehus [7], although their choice of *ansatz* was better-informed than Schrage's.

A few recent works have sought to validate the Schrage equation via molecular dynamics (MD) simulations of the classic two-surface problem of evaporation/condensation between two parallel liquid surfaces, typically spaced ∼10 mean free paths apart [8–10]. Yu and Wang [11] and Liang et al. [12] observed good agreement between the fluxes predicted by the Schrage equation and their MD simulations for evaporation/condensation of argon, as did Bird et al. [13] for *n*-dodecane. However, Chandra and Keblinski's [14] MD study of water found that the Schrage equation overpredicted heat and mass fluxes by ∼20%. These studies present an interesting quantification of the Schrage equation's applicability to the two-surface problem; however, the two-surface problem [8–10,15–20] is physically distinct from the half-space problem [8,15,21] and is thus treated differently in the kinetic theory literature. Graur et al. [22] recently used the S-model kinetic equation to quantify the inaccuracy of the Schrage equation and demonstrated that kinetic equations can provide similar accuracy to molecular dynamics and direct simulation Monte Carlo methods with significantly less computation time. However, this study was limited to the evaporation of monatomic fluids.

A large body of literature treats the half-space problem via various approximate solutions to the Boltzmann transport equation (BTE), thus explicitly conserving mass, momentum, and energy. These methods are more tedious than the classically cited treatment by Schrage, and the engineering community has largely preferred the Schrage equation, especially the approximate formulation derived by Nabavian and Bromley [23] and given in Carey's 1992 textbook [24]. This approximate formulation is attractive since it expresses the heat/mass flux of liquid–vapor

---

phase change as an explicit function of temperatures and pressures of the condensed and vapor phases. Further, it was derived for the low Mach number flow conditions typically seen in thermofluid engineering devices. Here, we revisit the Schrage equation through the lens of decades of kinetic theory literature and more recent experimental data to provide: (1) quantification of the accuracy of the Schrage equation for modeling evaporation and condensation; (2) an analysis of fundamentally accurate approaches for calculating heat/mass fluxes; and (3) recommendations for higher-accuracy estimations of evaporation/condensation fluxes.

2 Kinetic Theory Approach to Evaporation/ Condensation for a Planar Condensed Phase

2.1 General Theory. The kinetic theory describes the vapor phase using a molecular velocity distribution function, $f(\xi, x, t)$, which specifies the mass density of the gas in a differential volume of the molecular velocity space around velocity ξ at position x and time t. The local distribution function at a given set of spatial and temporal coordinates fully describes the local thermodynamic state and macroscopic flow velocity of the gas (see Appendix A). A stationary gas in thermodynamic equilibrium obeys the Maxwell–Boltzmann distribution

$$f_M(\xi) = \frac{\rho}{(2\pi RT)^{3/2}} \exp\left(-\frac{|\xi|^2}{2RT}\right) \tag{1}$$

This velocity distribution is specified by the mass density ρ, temperature T, and specific gas constant R of the vapor. In the analysis that follows, we consider single component systems (i.e., one species of a pure fluid) at a steady-state. For treatment of phase change kinetics between a planar liquid phase and its pure vapor, the vapor far from the liquid–vapor interface is assumed to reach an equilibrium state described by

$$f_v(\xi) = \frac{\rho_v}{(2\pi RT_v)^{3/2}} \exp\left(-\frac{|\xi - u_v|^2}{2RT_v}\right) \tag{2}$$

where the subscript "v" denotes properties of the equilibrium vapor flow in the far-field and u_v is the net velocity of the vapor stream. Commonly, the vapor phase is modeled as a semi-infinite half-space without flow tangential to the liquid surface, such that $u_v = u_v \hat{x}$, where $\hat{x}$ is the unit vector perpendicular to the liquid surface and pointing into the vapor phase (see Fig. 2).

At the liquid–vapor interface, the distribution function f_L is often split into a distribution function of molecules evaporated from the liquid (f_L^+) and a distribution function of vapor molecules incident on the liquid (f_L^-). The former is assumed to be the half-range Maxwellian distribution

$$f_L^+(\xi) = \frac{\rho_e}{(2\pi RT_L)^{3/2}} \exp\left(-\frac{|\xi|^2}{2RT_L}\right), \quad \xi_x > 0 \tag{3}$$

where ρ_e is the equilibrium density of the saturated vapor at the liquid temperature T_L (see Fig. 1 for illustration). One consequence of assigning Eq. (3) as a boundary condition is nonequilibrium (i.e., a discontinuity) at the liquid–vapor interface when net evaporation/condensation occurs. This loss of equilibrium is evident in that f_L can only be an equilibrium distribution function if $f_L^-(\xi) = f_L^+(\xi)$ for $\xi_x < 0$, which results in zero net velocity. The half-range Maxwellian form of f_L^+ has been corroborated via molecular dynamics simulations of monatomic [25,26] and polyatomic [27] species when T_L is well below the critical temperature. Frezzotti and Barbante also observed the half-range Maxwellian from their Enskog–Vlasov model calculations [28]. We note that other MD studies appear to contradict these findings [29–31], but the discrepancy appears to arise only from the choice of interphase boundary position. References [26] and [27] evaluated the distribution function at the center of the transition layer (the angstrom-scale region where the density transitions from liquid to vapor) while Refs. [30] and [31] explicitly chose a "vapor boundary" in the vapor region outside of the transition layer. In fact, Refs. [26] and [27] also evaluated the distribution function at points similar to those chosen by Refs. [30] and [31] and the results match well. Furthermore, nonequilibrium thermodynamic analysis has shown that the temperature of the liquid–vapor interface is very close to the temperature of the bulk liquid adjacent to the interface [32].

The net emitted flux may be smaller than predicted by Eq. (3) as a result of nonidealities at the liquid–vapor interface. To account for this effect, the evaporation coefficient $\hat{\sigma}_e$ is introduced such that the actual emitted distribution is $\hat{\sigma}_e f_L^+$ [21,26,33]. A similar allowance for diffuse reflection of a fraction of the condensing stream is made via the condensation coefficient, $\hat{\sigma}_c$. At equilibrium, Eq. (1) holds everywhere in the vapor, and therefore $\hat{\sigma}_e = \hat{\sigma}_c = \hat{\sigma}$ [21,24], with the latter often referred to as the "accommodation coefficient." The common practice extends this equality of evaporation and condensation coefficients to nonequilibrium analyses [21,34]; we will follow this precedent here under the caveat that this assumption is only certain to be accurate near
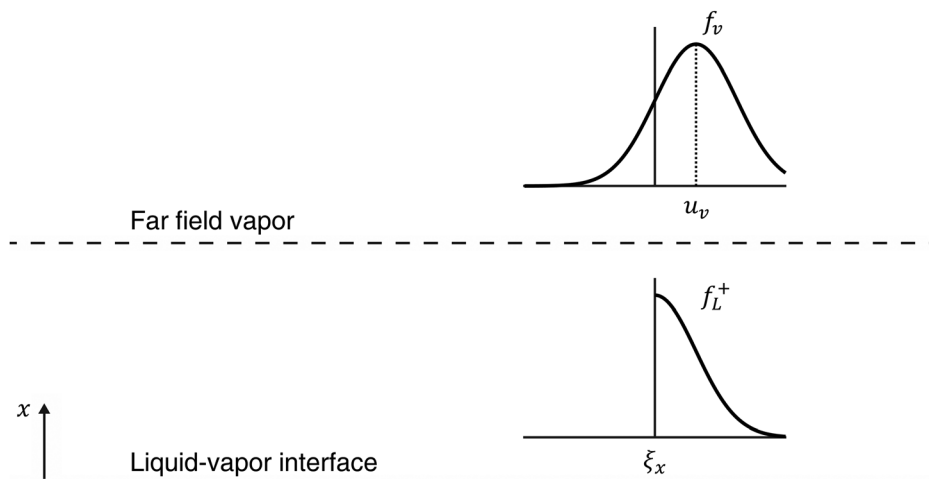
Fig. 1 Assumed forms of the velocity distribution function at the liquid–vapor interface (f_L^+) and in the far-field vapor (f_v). At the interface, the $\xi_x < 0$ portion of the distribution function (f_L^-) is unknown. Schrage approximated f_L^- as the $\xi_x < 0$ portion of f_v.

equilibrium, i.e., at low fluxes. The accommodation coefficient is a temperature-dependent property of a given fluid [5], bounded by 0 and 1. We note that the accommodation coefficient has a firm physical meaning, as described above, despite the fact that it is often treated as a fitting parameter for model equations. Much debate exists around the values of the accommodation coefficient for particular fluids (especially water) as it is very difficult to measure and likely highly sensitive to trace amounts of noncondensable gases in the vapor and impurities at the liquid–vapor interface. Accommodation coefficients for various fluids were compiled by Paul [35], and many studies on the accommodation coefficient of water were reviewed by Eames et al. [33]. More recent experimental measurements of the accommodation coefficient of water were briefly discussed by the authors [36].

Equations (2) and (3) are generally regarded as unquestionable boundary conditions for the half-space problem in the kinetic theory. However, the treatment of f_L^- varies among different analyses in the literature. Sections 2.2 and 2.3 will demonstrate that the treatment of f_L^- has a profound impact on the resulting model. From the fully specified velocity distribution functions at the liquid–vapor interface and in the far-field equilibrium region, the relationships among the state variables and the net evaporation/condensation flux can be found via control volume analysis, analogous to the Rankine–Hugoniot conditions for shock waves [37]. For the case of complete accommodation of a monatomic vapor, the conservation equations for mass, momentum, and energy are

$$\int_{\xi_x>0} \xi_x f_L^+ d\boldsymbol{\xi} + \int_{\xi_x<0} \xi_x f_L^- d\boldsymbol{\xi} = \rho_v u_v \tag{4a}$$

$$\int_{\xi_x>0} \xi_x^2 f_L^+ d\boldsymbol{\xi} + \int_{\xi_x<0} \xi_x^2 f_L^- d\boldsymbol{\xi} = \rho_v u_v^2 + \rho_v R T_v \tag{4b}$$

$$\int_{\xi_x>0} \frac{1}{2}|\boldsymbol{\xi}|^2 \xi_x f_L^+ d\boldsymbol{\xi} + \int_{\xi_x<0} \frac{1}{2}|\boldsymbol{\xi}|^2 \xi_x f_L^- d\boldsymbol{\xi} = \rho_v u_v \left(\frac{1}{2}u_v^2 + \frac{5}{2}RT_v\right) \tag{4c}$$

For polyatomic species, f_L must also be integrated over the internal energy space and the energy conservation expression (Eq. (4c)) changes to account for the transport of internal energy; examples can be found in Cercignani's textbook [38] and Barrett and Clement's article [5].

2.2 Schrage's Formula. Schrage assumed that the velocity distribution of molecules in the incident stream of vapor could be directly taken from the far-field distribution, that is

$$f_L^- = \frac{\rho_v}{(2\pi R T_v)^{3/2}} \exp\left(-\frac{|\boldsymbol{\xi} - u_v \hat{x}|^2}{2RT_v}\right), \quad \xi_x < 0 \tag{5}$$

This treatment was an important improvement over the Hertz-Knudsen formula for the half-space problem, which was derived in a similar fashion but did not account for the net velocity of the vapor. Substituting Eq. (5) into a slightly modified Eq. (4a) (to account for mass accommodation, see Appendix C), Schrage found the evaporating or condensing mass flux to be

$$J = \hat{\sigma}(2\pi R)^{-1/2}\left(\frac{p_e}{\sqrt{T_L}} - \Gamma\frac{p_v}{\sqrt{T_v}}\right)$$
$$\Gamma(S_v) = e^{-S_v^2} - S_v\sqrt{\pi}(1 - \text{erf}(S_v)) \tag{6}$$

where p_e is the equilibrium saturated vapor pressure at T_L and J is defined as positive for net evaporation. Γ is often called a "correction factor" that accounts for the net velocity in the vapor phase and is a function of the speed ratio $S_v = u_v/\sqrt{2RT_v}$, where $\sqrt{2RT_v}$ is the most probable thermal speed. Note that we have assumed ideal gas behavior to replace mass density with pressure

in Eq. (6). More detailed derivations of Eq. (6) can be found in Schrage's thesis [1] and Carey's textbook [24].

Inconveniently, Eq. (6) is an implicit expression for the mass flux (since $J \equiv \rho_v u_v$ and Γ is a function of u_v); thus, the fact that the speed ratio (which is of the same order as the Mach number) is quite small for typical engineering applications is often leveraged, leading to the simplification $\Gamma \approx 1 - S_v\sqrt{\pi} = \Gamma'$. After some manipulation, this approximation leads to [24]

$$J = \frac{2\hat{\sigma}}{2 - \hat{\sigma}}(2\pi R)^{-1/2}\left(\frac{p_e}{\sqrt{T_L}} - \frac{p_v}{\sqrt{T_v}}\right) \tag{7}$$

Equation (7) is widely used in the modeling of engineering systems, as it provides an explicit expression for the mass flux; in subsequent sections, we will refer to Eqs. (6) and (7) as the "Schrage equation" and the "explicit Schrage equation," respectively. Note that T_v and p_v are evaluated at the state of the gas in the continuum region adjacent to the liquid–vapor interface. For comparison, the Hertz-Knudsen formula is

$$J = \hat{\sigma}(2\pi R)^{-1/2}\left(\frac{p_e}{\sqrt{T_L}} - \frac{p_v}{\sqrt{T_v}}\right) \tag{8}$$

For complete accommodation ($\hat{\sigma} = 1$), Eq. (8) predicts only half the flux of Eq. (7). Ytrehus [21] noted that Eq. (7) is the more accurate expression for evaporation, except very close to the sonic condition.

For the sake of analysis, we nondimensionalize the macroscopic flow parameters as $T^* = T/T_L$, $p^* = p/p_e$, and $J^* = J/J_L^+$, where $J_L^+ = p_e/\sqrt{2\pi R T_L}$, the flux of evaporated molecules emitted from the liquid at $\hat{\sigma} = 1$. The dimensionless form of Eq. (7) is then

$$J^* = \frac{2\hat{\sigma}}{2 - \hat{\sigma}}\left(1 - \frac{p_v^*}{\sqrt{T_v^*}}\right) \tag{9}$$

Despite the widespread use of the Schrage equation in parts of the thermofluid engineering community [24,39–41], the kinetic theory community has pointed out flaws in Schrage's derivation that lead to an incorrect physical picture [5,21]. The root of the problem is the assumption that the distribution function of the incident stream is exactly the $\xi_x < 0$ portion of the shifted Maxwellian f_v (Eq. (2)), which is equivalent to assuming $f_v|_{\xi_x<0}$ describes the incident vapor stream as an infinitesimal distance away from the liquid surface. This condition entirely overlooks the transition from nonequilibrium at the liquid–vapor interface to the state of thermal equilibrium achieved in the far-field vapor. The transition region is known as the Knudsen layer (see Fig. 2), and only beyond this region is the gas described by the equilibrium distribution f_v [5,21].

While Schrage's choice of f_L^- is a reasonable first approximation, it neglects collisions between molecules of the incoming stream from the equilibrium region with molecules from the stream emitted from the liquid–vapor interface. This collision process enables relaxation of the nonequilibrium condition at the interface to the equilibrium state of the far-field vapor. The paradox of Schrage's physical picture is that he prescribes a nonequilibrium condition at the interface using a piece of the far-field equilibrium distribution, yet allows for no mechanism by which relaxation to the equilibrium state can be achieved (in fact, his kinetic models do not incorporate the collision integral from BTE).

As a result of this conceptual shortcoming, Schrage's derivation satisfies mass conservation (Eq. (4a)) but violates momentum and energy conservation at the liquid–vapor interface (Eqs. (4b) and (4c)). Barrett and Clement [5] mathematically demonstrated that the explicit Schrage equation violates energy conservation; however, the lack of explicit enforcement of momentum and energy conservation in the derivation of the Schrage expressions is sufficient to expect this conclusion. In fact, Schrage himself noted that
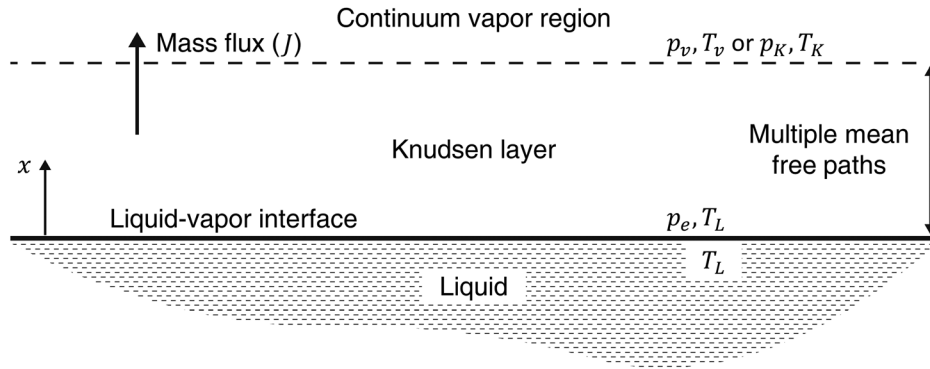
Fig. 2 Schematic diagram of the half-space problem of evaporation/condensation. The vapor is a semi-infinite domain in contact with a planar liquid surface, of which the temperature (T_L) is assumed to be known. Schrage considered the continuum vapor region to be in direct contact with the liquid–vapor interface, but the kinetic theory of gases requires that any perturbation from equilibrium causes the formation of a nonequilibrium Knudsen layer adjacent to the liquid–vapor interface. Collisions between vapor molecules in the Knudsen layer relax the nonequilibrium distribution at the interface to the shifted Maxwellian f_v in the continuum vapor region.

his choice of f_L^- "cannot possibly be a rigorous description of those molecules with $\xi_x < 0$ just at the phase interface" (adjusted to the notation in this work, Chapter V of Ref. [1]). Schrage proceeded to develop a mass flux expression by assuming instead $f_L^- = (1 - B\xi_x)f_L^+$, $\xi_x < 0$, where f_L^+, $\xi_x < 0$ indicates the same Maxwellian distribution as f_L^+, but for $\xi_x < 0$ instead of $\xi_x > 0$, and B is an arbitrary constant. This approach does allow for the conservation of mass, momentum, and energy, and it resembles the moment methods then in use for rarefied gas dynamics analysis and later applied to evaporation and condensation (see Secs. 2.3 and 4). However, we will not discuss this method further as we have not seen it used elsewhere in the literature and because a better choice of *ansatz* for f_L^- was introduced later.

In Secs. 2.3, 3.1, and 4, we will briefly introduce more rigorous analyses of the half-space problem developed in the kinetic theory community and discuss the ramifications of ignoring the Knudsen layer.

2.3 Knudsen Layer Treatment. Due to the nonequilibrium and subcontinuum nature of the Knudsen layer, it cannot be described by the Navier–Stokes equations [21,42]. Rather, the BTE is necessary to describe the evolution of the velocity distribution function

$$\frac{\partial f}{\partial t} + \xi_i \frac{\partial f}{\partial x_i} = I(f,f) \qquad (10)$$

where $I(f,f)$ is the binary collision integral which is described in detail in the literature [21,37,42]. The boundary conditions for the half-space problem are f_L^+ and f_v (as specified in Sec. 2.1) at the interface and at the equilibrium edge of the Knudsen layer, respectively. The thickness of the Knudsen layer is not known a priori, but analysis of the BTE shows that its thickness scales with the mean free path of the gas phase (λ, average distance gas particles travel between collisions). In contrast to Schrage's analysis, f_L^- is a result of solving the BTE subject to the half-space boundary conditions, rather than a boundary condition to be enforced. The BTE is difficult to solve for practical problems due to the complicated nature of the collision integral [38]; however, decades of theoretical and experimental work have led to a variety of approximate solution methods.

As previously discussed in the literature, the half-space problem for a given vapor species is fully characterized by three parameters: the pressure ratio p_K^*, temperature ratio T_K^*, and Mach number $M_K = u_K/\sqrt{\gamma R T_K}$ [21,42,43], where γ is the ratio of specific heats.

Focusing our analysis on the temperature range where vibrational excitation can be neglected, γ relates to the number of rotational degrees-of-freedom (j) as $\gamma = (5+j)/(3+j)$. As illustrated in Fig. 2, we use the subscript "K" instead of "v" to denote parameters evaluated at the equilibrium edge of the Knudsen layer to stress that these parameters are boundary conditions for the continuum region. The standard approach is to treat the Knudsen layer problem in the half-space framework and then couple the Knudsen layer solution to the continuum region. We briefly discuss this coupling in sec. 5. As heat and mass fluxes are of more interest than the Mach number for most engineering applications of liquid/vapor phase change, we will refer to the dimensionless flux as the third parameter, rather than the Mach number (the two are related by the expression $J^* = \sqrt{2\pi\gamma}M_K p_K^*/\sqrt{T_K^*}$).

The problem of weak (or low Mach number) evaporation/condensation has been solved using linear perturbation theory [8,44,45]. To describe strong evaporation, Anisimov [6,46] applied a moment method based on the collision-invariant moments of the BTE (i.e., mass, momentum, and energy), adapting methods developed for the study of the shock wave structure. Ytrehus [7] developed this moment method further and with Alvestad [47] extended it to condensation. Shankar and Marble [48] also treated the half-space problem using a similar moment analysis, but their approach only provided a steady solution for condensation. Moment methods require certain assumptions to be made about the incident stream, yet these assumptions are much looser than Schrage's and, importantly, allow the simultaneous conservation of mass, momentum, and energy. The BGK method (developed by Bhatnagar, Gross, and Krook [49] and Welander [50]) is widely used as a starting point to achieve analytical/numerical solutions to the BTE by approximating the collision integral as $I(f,f) \rightarrow \nu_c(f_M - f)$, where ν_c is the characteristic collision frequency and f_M is the local Maxwellian described by the local temperature, density, and macroscopic velocity of the gas. This model is sometimes referred to as the "relaxation time approximation" as $1/\nu_c$ is a timescale over which f relaxes to the local Maxwellian via collisions.

Several numerical methods have been developed to solve the BGK approximation of the BTE for the half-space problem [51,52]. These numerical models require no additional assumptions about the form of f_L^-, and have thus been used to validate the moment methods, which have the advantage of offering closed-form analytical solutions. Numerical solutions to the BGK equation have been developed to the point of describing monatomic and polyatomic gas species, but they are not capable of accounting for any further properties specific to the species in question. Direct

simulation Monte Carlo (DSMC) solutions provide the most precise description of the half-space problem owing to the development of collision models that do not require the relaxation time approximation. Further, these collision models have parameters that can be tuned to replicate the experimentally determined viscosity particular to unique gas species (see Bird [53,54] for a detailed description of the DSMC method and its collision models). DSMC calculations for hard-sphere gases, numerical methods using the relaxation time approximation, and the moment method all provide consistent mass flux calculations for the half-space problem for evaporation [43] and condensation [55].

Ytrehus [21] provided simple guidelines for selecting the appropriate model for the half-space problem according to the magnitude of the dimensionless driving pressure, $\Delta p^* = (p_e - p_K)/p_e$. The weak mass transfer regime is described by $|\Delta p^*| \ll 1$ and is appropriately described by the linear perturbation theory solutions. Strong mass transfer occurs when $|\Delta p^*| \sim 1$ and should be modeled using the moment methods, high-order numerical approximations (e.g., numerical solutions to the BGK equation), or DSMC. Problems of moderately strong mass transfer ($|\Delta p^*| < 0.1$) can alternatively be modeled using a linearized solution to the moment methods that will be discussed in Sec. 4.

The existing kinetic theory literature describes some key differences between the descriptions of evaporation/condensation from BTE analysis and Schrage's equation. Recalling Eq. (9), Schrage's explicit dimensionless flux expression for both evaporation and condensation, we see that Schrage's analysis states that both the dimensionless temperature and pressure must be specified to determine the nondimensional flux. In contrast, the BTE-based methods all agree that only one of these can be a free parameter for evaporation: e.g., $T_K^* = T_K^*(p_K^*)$, $J^* = J^*(p_K^*)$, etc., as already discussed. On the other hand, the BTE methods do show that condensation requires two parameters to be specified; this fundamental difference between evaporation and condensation is not captured by the Schrage equation. Furthermore, Ytrehus showed that the explicit Schrage equation (Eq. (7)) overestimates the dimensionless flux in the case of $\hat{\sigma} = 1$ [21].

3 Quantification of Error From the Schrage Equation

We believe that it would be valuable to the community to provide quantitative examples of the deviations in fluxes calculated using the Schrage equation (both in full and explicit form) from theoretically accurate values for common engineering problems. In this section, we describe a numerical method from the literature for approximately solving the BTE for polyatomic gases and compare fluxes calculated from this method to calculations using the Schrage equation. Much of this analysis is performed for evaporation and condensation of water at low temperatures (0–100 °C), but also show that these insights apply to other fluids and different operating conditions.

3.1 Numerical Method for Evaporation/Condensation of Polyatomic Vapor.
After searching the literature for suitable high-fidelity models for the kinetics of evaporation/condensation of water, we selected the numerical methods of Frezzotti for evaporation [43] and Frezzotti and Ytrehus for condensation [55]. Both of these methods are applicable to polyatomic vapor. Their solution of a BGK-like equation by finite differences provides pressure curves and mass flux calculations that agree very well with DSMC calculations for hard-sphere gases, where the Borgnakke–Larsen model [56] was used to account for the rotational degrees-of-freedom of polyatomic gases. For a polyatomic gas, they considered a modified distribution function in one spatial dimension, $f'(\nu, \epsilon | x, t)$, which describes the molecular velocity and rotational energy ϵ at location x and time t (Eq. (10) still holds under this framework). They then applied the BGK-like collision operator developed by Holway [57]

$$I(f', f') = \nu_{el}(n, T_t)(\Phi_{el} - f') + \nu_{in}(n, T_t)(\Phi_{in} - f') \qquad (11)$$

where ν_{el} and ν_{in} are the elastic and inelastic collision frequencies, n is the number density of molecules having rotational energy ϵ, T_t is the translational temperature, and Φ_{el} and Φ_{in} are the "frozen" local equilibrium and local equilibrium Maxwellian distribution functions, respectively. Expressions for each of these terms can be found in Appendix B1, but it should be noted here that the collision frequencies are calculated from the shear viscosity of a hard-sphere gas, rather than using the temperature-independent collision frequency of Maxwell molecules used elsewhere in the literature [15,51]. We applied a numerical method similar to that developed by Frezzotti [43] using the second-order finite difference discretization scheme described by Kazuo et al. [51] to solve Eq. (10) with the collision operator of Eq. (11). Details can be found in Appendix B2.

We found that our numerical solver could reproduce the same relationships among pressure ratio, temperature ratio, and Mach number as the original references for evaporation [43] and condensation [55] of polyatomic gases (see Appendix B4). Further, our results for monatomic gases matched those computed by Sone [15]. However, we note that the formulation is incapable of differentiating between species that have the same number of rotational degrees-of-freedom [43]. Thus, to validate the application of this analysis to the common engineering problem of evaporation/condensation of water, we compared our numerical results to the experimental results and DSMC calculations of Lu et al. [58]. They used the variable soft sphere collision model with parameters that replicate the viscosity of water vapor, meaning their results are specifically accurate for water. Our present model matches their DSMC and experimental results very well (see Appendix B4), suggesting the hard-sphere model and relaxation time approximation offer sufficient accuracy for real gases.

The simplifications to the collision term of the Holway model result in a kinetic description that distinguishes between species only by their number of rotational degrees-of-freedom. Recalling that evaporation of a pure fluid is fully described by one dimensionless parameter (p_K^*, T_K^*, or J^*), the Holway model provides a single curve per specified j relating any two parameters to each other. That is, the relation $J_{j=0}^* = J^*(p_K^*)_{j=0}$ is universal for monatomic species and separate relations exist for diatomic ($j = 2$) and nonlinear polyatomic ($j = 3$) species. In the case of condensation, there is a two-dimensional parameter space per value of j (i.e., $J_{j=0}^* = J^*(p_K^*, T_K^*)_{j=0}$). To reduce the parameter space, it is useful to consider the case where p_K^* and T_K^* are not independent parameters but rather are constrained by the saturation relation of the fluid, i.e., the vapor is in a saturated state, a widely relevant condition in engineering applications [24,59–61]. When this special case is considered, each fluid has a unique relation ($J^*(p_K^*)$ or $J^*(T_K^*)$) corresponding to its saturation curve. Schrage's analysis of the case of a saturated vapor state provides fluid-specific solutions for both evaporation and condensation, with the former being an erroneous outcome as evaporation should be described by one parameter only.

This analysis of the Schrage equation's accuracy first considers water with $T_L = 25$ °C and a saturated vapor state as a case study and then briefly discusses how these results can be applied to other fluids and operating conditions, including nonsaturated states. Here we show the solutions as functions of the dimensionless driving pressure (Δp^*) as has been done by others [21,55,58].

3.2 Results for Water With Complete Accommodation.
We first study the accuracy of the Schrage expressions for evaporation/condensation of water assuming full accommodation ($\hat{\sigma} = 1$). As water is a nonlinear, polyatomic fluid, we used $j = 3$ for the Holway model. The properties of water at $T_L = 25$ °C and $T_K = T_{sat}(p_K)$ were used as inputs for the Schrage expressions, the condensation ($J^* < 0$) portion of the Holway results, and the dimensional axes, where the superheat is defined as $\Delta T = T_L - T_{sat}(p_K)$. Figure 3 compares the relation between flux and dimensionless driving pressure predicted by Eqs. (6) and (7) to the Holway model results. As described in Sec. 3.1, the Holway
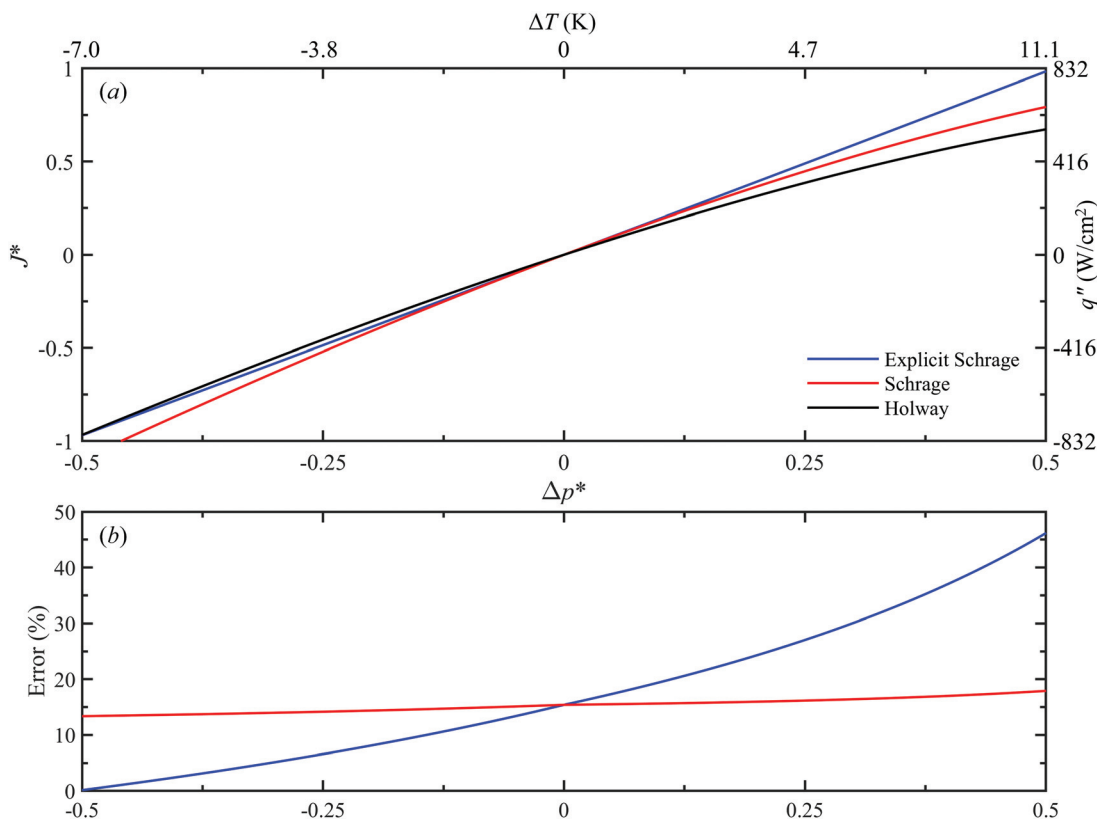
Fig. 3 Error quantification for using the Schrage expressions to model evaporation and condensation of water with $T_L = 25\,°C$. The Schrage equation (Eq. (6)) overpredicts evaporation ($J^* < 0$) and condensation ($J^* > 0$) fluxes by ~15% across the range of conditions shown here. Interestingly, the explicit Schrage equation (Eq. (7)) increasingly overpredicts the evaporation flux as the flux increases, but is more accurate than Eq. (6) for the weak to moderate condensation regime shown here. Relative errors greater than zero signify overprediction of flux for both evaporation and condensation following the definition prescribed in Eq. (12), where the Holway model is the reference here. The dimensional superheat and heat flux are determined using the saturation properties of water with $T_L = 25\,°C$. Both the dimensionless and dimensional abscissae of (a) and (b) are identical. The abscissae represent linear increments in Δp^* but not superheat values due to the nonlinearity of the saturation relation.

model curve for evaporation ($J^* > 0$) applies not only to water but any fluid with three internal degrees-of-freedom. We defined relative error as

$$\text{Error} = \frac{Q_{\text{mod}} - Q_H}{Q_H} \qquad (12)$$

where Q is a calculated quantity the subscripts "mod" and H denote calculations from the model in question and the Holway model, respectively. This error definition is used consistently throughout this work and has the property of being positive when Q_{mod} overpredicts the absolute value of the quantity, e.g., the flux error is positive when J^*_{mod} overpredicts the net evaporation or net condensation rate. Consistent with previous studies, the explicit Schrage equation overpredicts the evaporative flux [21]. The full expression (Eq. (6)) overpredicts the evaporative flux to a lesser degree and consistently overpredicts the flux by ~15% for both evaporation and condensation across the range considered here (Fig. 3(b)). Interestingly, Eq. (6) is less accurate than the explicit expression for condensation. This trend of the explicit expression performing better for condensation and worse for evaporation is a coincidence resulting from the fact that Γ' is always less than Γ (see Appendix C), artificially shrinking the contribution of the condensing stream and thus resulting in $J^*_{\text{Eq.(6)}} < J^*_{\text{Eq.(7)}}$. Observing that Eq. (6) always overpredicts the absolute value of the flux, this inequality means that the approximation of Γ' can help to offset the inaccuracy of Eq. (6) under net condensation but exaggerates this inaccuracy under net evaporation.

3.3 Effect of the Accommodation Coefficient. Although the accommodation coefficient of water is debated in the literature, it is often reported to be significantly less than unity [33,35]. Conveniently, the Schrage expressions offer straightforward consideration of the accommodation coefficient with Eq. (7) remaining an explicit expression. Accommodation can be directly accounted for in the numerical Holway solver (see Appendix B) at an additional computational expense, or the solution for full accommodation can be transformed [16,21,52] as

$$p_K^{*-1} = (p_K^*)_{\hat{\sigma}=1}^{-1} + \frac{1-\hat{\sigma}}{\hat{\sigma}} 2\sqrt{\frac{\pi}{T_K^*}} S_K \qquad (13)$$

where $(p_K^*)_{\hat{\sigma}=1}$ is the pressure ratio corresponding to the model results calculated with complete accommodation. We note that Eq. (13) was derived assuming fully diffuse reflections. Conceptually, Eq. (13) maps the pressure ratio of a real fluid to that of a pseudo-fluid with the property $\hat{\sigma} = 1$ such that $S_K(p_K^*) = S_K((p_K^*)_{\hat{\sigma}=1})$ and $T_K^*(p_K^*) = T_K^*((p_K^*)_{\hat{\sigma}=1})$. Therefore, the relations among these parameters need only be calculated for complete accommodation, then the dataset can be transformed to describe an arbitrary value of $\hat{\sigma}$ by replacing the pressure ratio with Eq. (13) at virtually no computational expense compared to the numerical Holway solver. While this method incurs no error for evaporation, transforming condensation calculations causes $T_K^*(p_K^*)$ to deviate from the saturation relation initially enforced in the complete accommodation calculation. However, the condensation flux is only weakly dependent on T_K^* when holding p_K^*
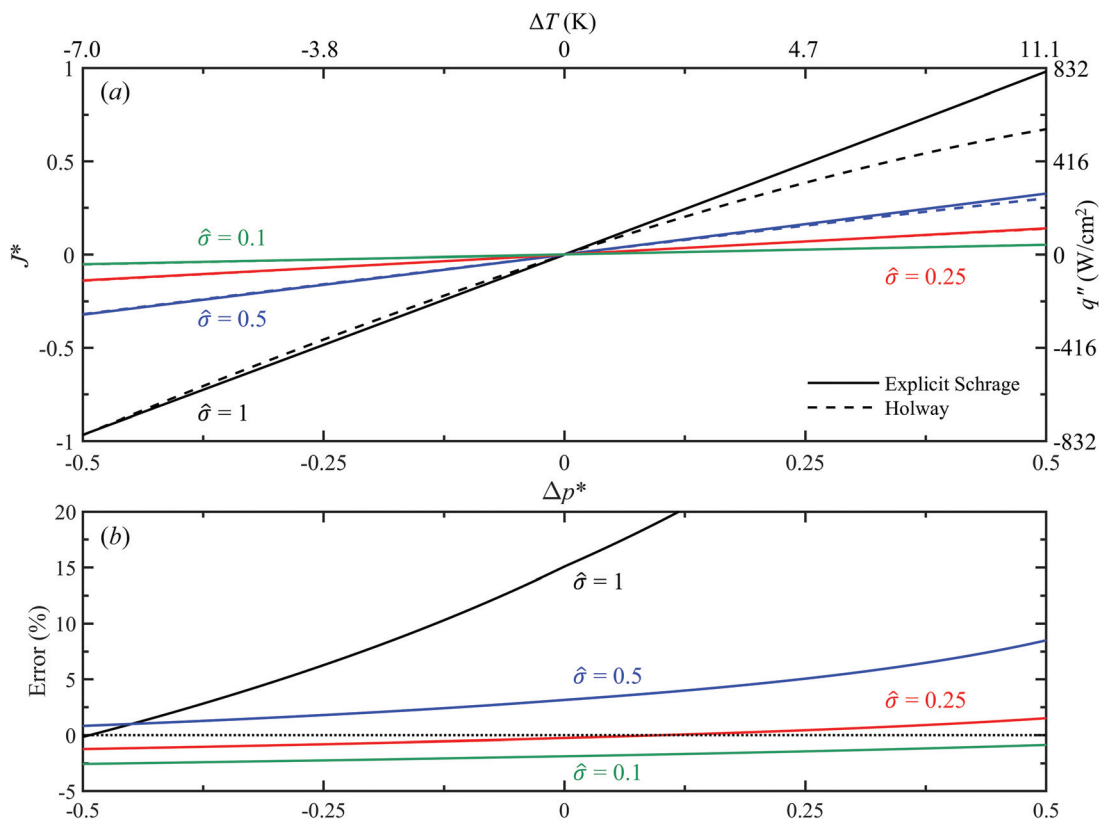
Fig. 4 Effect of the accommodation coefficient on the accuracy of the explicit Schrage equation (Eq. (7)) for water with $T_L = 25\,°C$. The explicit Schrage equation matches the Holway model results better at lower values of the accommodation coefficient for evaporation and condensation, see the overlapping dashed and solid lines for $\hat{\sigma} = 0.1, 0.25$ in (*a*). For water, many experimental studies have reported $\hat{\sigma} < 0.5$, in which case Eq. (7) is accurate within 10% for the range shown here. The top (ΔT) and bottom (Δp^*) abscissae of (*a*) and (*b*) are identical, and the dimensional superheat and heat flux are determined using the saturation properties of water with $T_L = 25\,°C$. The dotted line in (*b*) is a guide to the eye for zero relative error.

constant. We calculated the relative error incurred by assigning constant temperature ratios $T_K^* = T_{\text{sat}}^*(\Delta p^* = 0) = 1$ or $T_K^* = T_{\text{sat}}^*(\Delta p^* = -0.5) = 1.023$ instead of using the saturation relation to calculate the condensation flux of water at $T_L = 25\,°C$ from $-0.5 \leq \Delta p^* < 0$ for complete accommodation. We found the error caused by slightly deviating from the saturation curve to be $\approx 1\%$ at most (see Appendix D).

Figure 4 compares the explicit Schrage equation predictions to the Holway model calculations for the same conditions as Fig. 3 but with varying values of $\hat{\sigma}$. The Schrage expression properly captures the trend that decreasing $\hat{\sigma}$ suppresses the flux of net evaporation and condensation. We observe that the explicit Schrage equation is much more accurate for $\hat{\sigma} < 1$ than for full accommodation; this finding agrees well with the observation of Lu et al. [58] that their experimental data for evaporation of water into its pure vapor could be described well by DSMC calculations or the explicit Schrage equation with the same $\hat{\sigma} = 0.31$. However, our data show that the relative error does not converge to zero as $\hat{\sigma} \rightarrow 0$, but rather that Eq. (7) can underpredict the flux for sufficiently small values of $\hat{\sigma}$ (Fig. 4(*b*)). We found that Eq. (6) shows the same trend with $\hat{\sigma}$ as Eq. (7).

3.4 Ramifications for Practical Use of the Schrage Equation. Despite speculation that the full, nonlinear Schrage equation (Eq. (6)) would not suffer from the same inaccuracy widely attributed to the more popular explicit form (Eq. (7)) [12,14], our results show that Eq. (6) still fails to accurately describe the kinetics of evaporation and condensation. This failure can be attributed to the lack of enforcement of momentum and energy conservation in Schrage's derivation, allowed by neglecting molecular collisions and setting the incident stream to the $\xi_x < 0$

portion of the far-field vapor distribution function. With quantification and cause of its inaccuracy, the question remains: under what conditions has Schrage's approximation given reasonable accuracy despite its flaws? The answer ought to lie in the accommodation coefficient. As shown in Fig. 4(*b*) the error of the explicit Schrage expression (and Eq. (6) as well) is relatively low for fluids with small $\hat{\sigma}$. Polar fluids like water and alcohols typically fall into this range, and these fluids are perhaps the most well-studied [24,35,62]. Furthermore, $\hat{\sigma}$ is a difficult property to measure accurately, and the literature reflects much disagreement about its value, particularly for polar fluids like water [33–35]. Thus, $\hat{\sigma}$ is often treated as a fitting parameter in evaporation/condensation experiments [35,58,63–65]. Because the Schrage expressions overestimate the flux when the true $\hat{\sigma}$ of the fluid is large ($\hat{\sigma} \gtrsim 0.5$, from Fig. 4), a reasonable value of $\hat{\sigma}$ (i.e., bounded by 0 and 1) for Eq. (6) or Eq. (7) can always be fitted to experimental data. For instance, we performed nonlinear least squares regressions to fit the Schrage expressions to the same $\hat{\sigma} = 1$ curve for the Holway model as shown in Fig. 3(*a*). Using $\hat{\sigma} = 0.94$, the Schrage equation predicts the $\hat{\sigma} = 1$ Holway curve with less than 10% error and even better accuracy for low flux conditions (Fig. 5). In practice, $\hat{\sigma}$ is unlikely to be fit to data spanning such a large range of condensation and evaporation conditions; rather, the experimental data is likely to cover either condensation or evaporation for a limited set of flux conditions [35,58,63–65]. In this case, it is likely that fitting $\hat{\sigma}$ will reasonably reproduce the data within the bounds of uncertainty. For example, considering the $\hat{\sigma} = 1$ curve for the Holway model (Fig. 3(*a*)) restricted to evaporative fluxes from 0–100 W/cm² (for water at $T_L = 25\,°C$) results in less than 0.5% and 2% error from Eqs. (6) and (7), respectively.
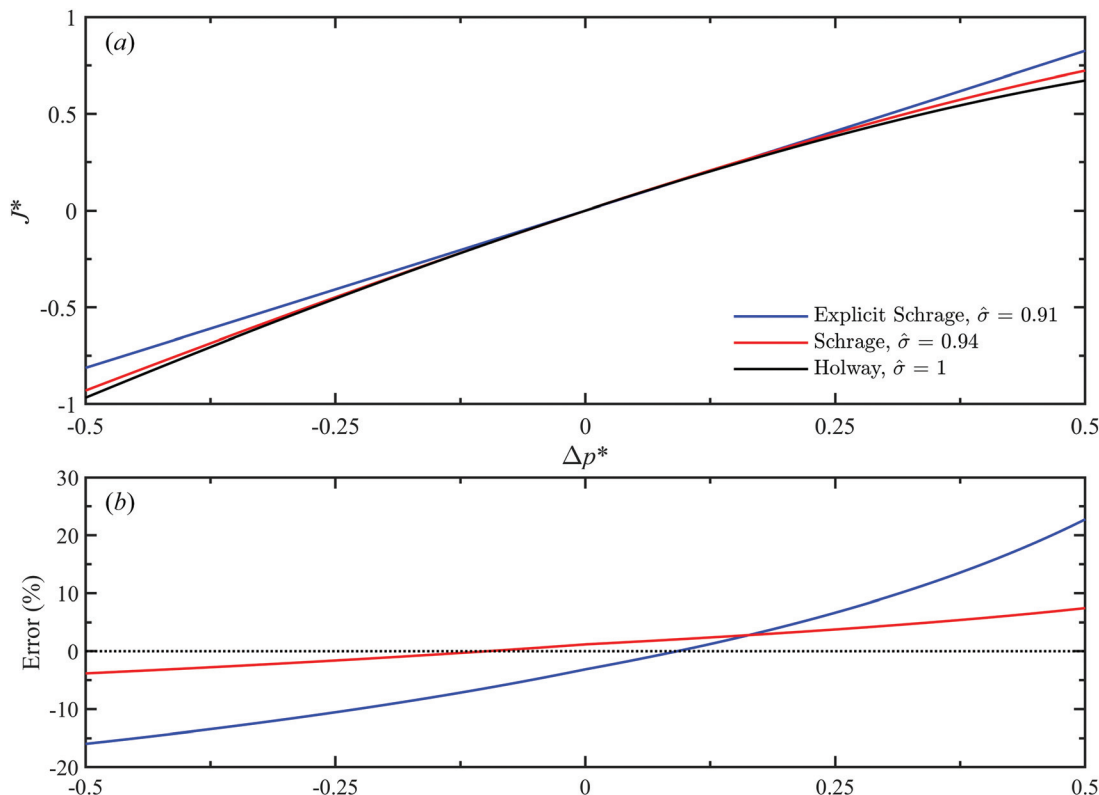
Fig. 5 Nonlinear least-squares fittings of the Schrage expressions to the Holway model data for water with $T_L = 25\,°C$ and complete accommodation. Fitting artificially low values of $\hat{\sigma}$ significantly improves the accuracy of both equations. The dotted line in (b) is a guide to the eye for zero relative error.

3.5 Extension to Other Operating Conditions and Fluids. While the dimensionless relation between flux and driving pressure for evaporation of a fluid with $j = 3$ applies to any absolute T_L, the relation does not strictly hold for condensation for different T_L values or different working fluids as the saturation relation varies. We calculated the condensation flux relations for water at $T_L = 1\,°C$ and $T_L = 100\,°C$ and found that the relation $J^*(\Delta p^*, T_K^*|_{\text{sat}}; T_L = 25\,°C)$ from Fig. 3(a) deviates by less than 0.2% and less than 0.5% from $J^*(\Delta p^*, T_K^*|_{\text{sat}}; T_L = 1\,°C)$ and $J^*(\Delta p^*, T_K^*|_{\text{sat}}; T_L = 100\,°C)$, respectively (see Appendix D). Furthermore, fixing either $T_K^* = 1$ or $T_K^* = 1.023$ for $T_L = 25\,°C$, rather than using the saturation curve, results in a maximum error of $\sim$1%, as discussed in Sec. 3.3. Thus, we infer that the condensation flux of water is only weakly dependent on T_K^* in this range and saturated conditions for $1\,°C \leq T_L \leq 100\,°C$ and that condensation flux can be accurately modeled using any single calculated flux relation, e.g., the data shown in Fig. 3(a). Recalling the dimensionless form of the explicit Schrage equation (Eq. (9)), we see that the Schrage equations are also only weakly dependent on T_L for the same range since T_v^* (using the Knudsen-layer ignorant notation) is very close to unity. It follows that the error in flux prediction at other T_L in this range should be like that of Fig. 3(b).

Other fluids with $j = 3$ have condensation flux relations that differ from water only by their saturation relations. We also calculated the flux relation with $T_K^* = 1.1$ fixed and observed less than 5% deviation from the curve for saturated water at $T_L = 25\,°C$ (Appendix D). This represents a relatively extreme case: for saturated water at $T_L = 25\,°C$ this corresponds to $\Delta p^* = -3.9$. As for monatomic ($j = 0$) and diatomic ($j = 2$) species, we found that the evaporation and condensation fluxes deviate little from the $j = 3$ case (Appendix D). This result agrees well with Frezzotti and Ytrehus [55], who found that J^* as a function of Δp^* calculations for different values of j collapse to a single curve for condensation at the same T_K^*. We note here that the choice of normalizing by the mass flux emitted from the liquid (J_L^+) is justified by this result: J^* is not independent of j if its normalization involves the

sonic speed (which depends on j via the ratio of specific heats). Synthesizing these observations about the dependence of the dimensionless flux on T_K^* and j, the results of Fig. 3 provide a reasonable understanding of the general accuracy of the Schrage equations. For example, we calculated the flux relation for argon using $T_L = 100\,K$ for the condensation curve and compared this result with the Schrage equations (Fig. 6). The error of the Schrage equations for argon is nearly identical to their error for water.

4 Discussion of Alternative Models

Implementation in practical engineering design requires a model that is either analytical or numerical with a low computational cost. The highest-fidelity models such as DSMC and our finite difference solver for the Holway model do not meet this level of computational efficiency. Thus, we believe it is worthwhile to use our highly accurate numerical method to evaluate simpler BTE-based models that could be used in place of the fundamentally flawed Schrage expressions. The moment method proposed by Anisimov [6] and further developed by Ytrehus [7] has been shown to compare very well to molecular dynamics, DSMC, numerical solutions to the BGK equations, and the S-model kinetic equation [21,22,66]. Inspired by Mott-Smith's [67] model for a strong shock wave, Anisimov [6] proposed a trimodal *ansatz* to describe the distribution function for the half-space evaporation problem of monatomic species:

$$f(x, \xi_x) = a_L^+(x) f_L^+(\xi_x) + a_K^+(x) f_K^+(\xi_x) + a_K^-(x) f_K^-(\xi_x) \quad (14)$$

where $f_K^+(\xi_x)$ and $f_K^-(\xi_x)$ are the $\xi_x > 0$ and $\xi_x < 0$ portions of Eq. (2), with the subscript "v" once again replaced by "K." It can readily be seen that the required boundary conditions at the interface and Knudsen layer boundary described in Sec. 2.1 are satisfied by choosing

$$
\begin{aligned}
a_L^+(0) &= 1, \quad a_K^+(0) = 0 \\
a_L^+(\infty) &= 0, \quad a_K^+(x \to \infty) = a_K^-(x \to \infty) = 1
\end{aligned}
\quad (15)
$$
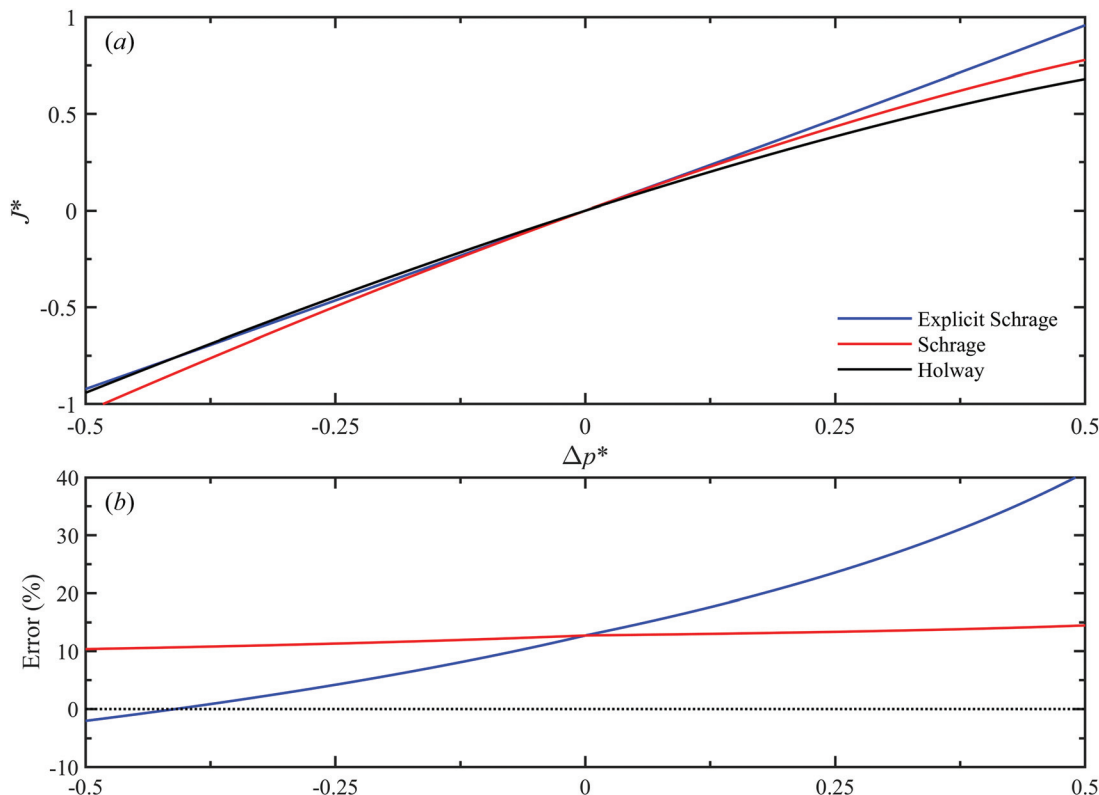
Fig. 6 Error quantification for using the Schrage expressions to model evaporation and condensation of argon with $T_L = 100$ K. The error of both equations is similar to that of the case of water with $T_L = 25\,°C$, with a slight shift away from overpredicting fluxes. The Holway model is used as the reference for the relative error in (b), where the dotted line is a guide to the eye for zero relative error.

Here, we have used "$x \to \infty$" to reflect the fact that the Knudsen layer problem is solved without regard to any continuum flow region, i.e., the distribution function tends asymptotically to Eq. (2) as x goes to infinity. Conceptually, Eq. (14) approximates the distribution function at any point in the Knudsen layer as a weighted combination of the distribution functions that are known at the boundaries. Following Ytrehus [21], Eqs. (14) and (15) can be substituted into Eqs. (4) to satisfy the conservation of mass, momentum, and energy across the Knudsen layer. We additionally followed Cercignani's method [38,68] of accounting for internal degrees-of-freedom in the energy balance expression (Eq. (4c)) for a more accurate description of polyatomic vapor. The three-moment equations for evaporation are shown in the dimensionless form in Appendix E (Eqs. (E1)–(E3)). This analysis provides three equations for the unknown value $a_K^-(0)$ and two of the three macroscopic flow variables p_K^*, T_K^*, and M_K^*; thus, one of the macroscopic flow variables specifies the entire problem, as discussed in Sec. 2.1.

The same trimodal *ansatz* cannot be applied to the problem of half-space condensation two of the macroscopic flow variables must be specified in that case. Thus, Ytrehus and Alvestad [47] introduced a fourth mode, $a_4^-(x)f_4^-(\xi_x)$, representing the molecules reflected back toward the interface as a result of the first collisions of the evaporated molecules, where $f_4^-(\xi_x)$ is a known distribution calculated from the BGK model. $f_4^-(\xi_x)$ and the three conservation equations for condensation using four modes are shown in Appendix E (Eqs. (E8)–(E10)). The fourth mode adds additional unknown to the control volume analysis, $a_4^-(0)$, thus requiring that two of the macroscopic flow variables be specified to describe the problem. As we are unaware of any extension of the moment method to condensation of polyatomic species [55], our moment method calculations for net condensation do not distinguish species by internal degrees-of-freedom. These same analyses for evaporation and condensation can be applied to fluids

with arbitrary $\hat{\sigma}$ via Ytrehus' transform [21] by substituting all p_K^* terms in the conservation equations with the $(p_K^*)_{\hat{\sigma}=1}$ expression that results from rearranging Eq. (13). Therefore, the flux relation for evaporation/condensation of any fluid can be approximated by numerically solving the corresponding system of equations (at a very small computational cost compared to the Holway model).

These moment equations for evaporation and Eq. (13) can be linearized (see Refs. [21] and [38]) and simplified into an analytical expression for the evaporation flux with arbitrary $\hat{\sigma}$, resulting in

$$J^* = \frac{\omega\hat{\sigma}}{\hat{\sigma} + (1 - \hat{\sigma})\omega}\Delta p^* \tag{16}$$

$$T_K^* = 1 - \frac{\hat{\sigma}}{8/\omega + (1 - \hat{\sigma})\omega'}\Delta p^* \tag{17}$$

where $\omega = 32\pi/(32 + 9\pi)$ and $\omega' = (23\pi - 32)/4\pi$.

We compare the flux prediction performance of the moment method, Eq. (16) (L. moment method), and the explicit Schrage equation (Eq. (7)) to the Holway model in Fig. 7. Here we considered a monatomic species with $T_K^* = 1$ fixed in the net condensation regime. This moment method reproduces the Holway model flux calculations with high accuracy: within 0.4% and -4% for evaporation and condensation, respectively. The discontinuity of the relative error of the moment method at $\Delta p^* = 0$ results from the additional approximation of the fourth mode required for condensation. The linearized moment expression outperforms the explicit Schrage equation in predicting the evaporative flux and the lower condensation flux regime. Equation (16) is an especially good choice of model for low flux evaporation/condensation, providing less than ±5% error in the range $-0.1 < \Delta p^* < 0.1$. This behavior is expected as Eq. (16) is an expansion of the highly accurate moment method around the equilibrium (zero flux)
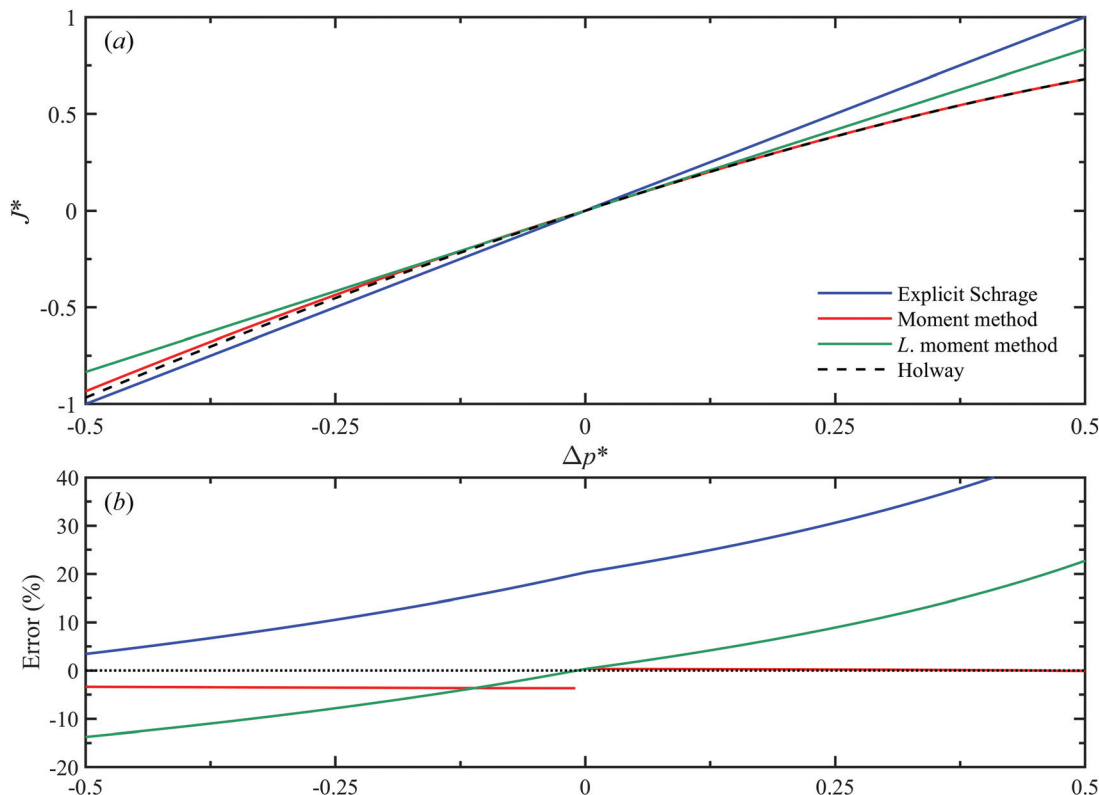
Fig. 7 Comparison of the explicit Schrage equation (Eq. (7)), moment method, and linearized moment method (Eq. (16), *L*. moment method) for monatomic fluids with complete accommodation and $T_K^* = 1$ fixed for the condensation calculations. The moment method deviates less than 0.4% and less than 4% from the Holway model for evaporation and condensation, respectively. Equation (16) is especially accurate for low fluxes and outperforms Eq. (7) for evaporation and low flux condensation. The dotted line in (*b*) is a guide to the eye for zero relative error.

condition. On the other hand, the Schrage expressions do not have the guarantee of being especially accurate at low fluxes, as can be seen in Fig. 3. Along with this contrast, Eq. (16) is comparable to the explicit Schrage equation in complexity (both are explicit, linear in Δp^*, and facilitate computation for any value of $\hat{\sigma}$), making it a particularly attractive substitute for Eq. (7) in computational fluid dynamics (CFD). We also observed that, like the Schrage expressions, the moment method and its linearized formulation tend to increase in accuracy as $\hat{\sigma}$ decreases (Appendix E2). We also analyzed the accuracy of using the moment method and Eq. (16) for a polyatomic fluid with $j = 3$. As one would expect following our observation in 3.5 that the flux is impacted little by internal degrees-of-freedom, we found that the relative errors of these two models increase marginally compared to the data in Fig. 7(*b*). For example, the maximum error of the moment method for evaporation increases to 1% (see Appendix E2).

We note that applying Eq. (16) to condensation is physically flawed as it describes the flux as a function of Δp^* only when T_K^* should be an additional parameter. However, Ytrehus' discussion [21] of linearization shows that the temperature ratio drops out of the mass flux expression, even for condensation. This finding is in agreement with our analysis in Sec. 3.5: our data shows that the condensation flux has a weak dependence on T_K^*. Further, the use of Eq. (16) to model net condensation seems no more inappropriate than the use of the Schrage expressions for evaporation, where the specification of both Δp^* and T_K^* is physically flawed. Equation (16) outperforms the explicit Schrage equation for $\Delta p^* \gtrsim -0.3$.

5 Coupling to Continuum Vapor Flow

5.1 The Role of the Knudsen Layer in Practical Systems. As noted in Sec. 2.3, solving the BTE for the half-space problem

provides boundary conditions for the continuum region, in which the Navier–Stokes equations aptly describe the flow. In engineering applications, complicated modeling (such as two-phase CFD) may be needed for the liquid and the continuum vapor region. It is useful to regard p_K^*, T_K^*, and J^* (or M_K) as jump conditions that form the boundary conditions at the interface for the Navier–Stokes equations. Here we assume that the system has a continuum region after the Knudsen layer, requiring that the characteristic length scale (d) is much larger than the mean free path (i.e., that the Knudsen number Kn $\equiv \lambda/d$ is small). We note that d should be taken as a geometric length scale or macroscopic boundary layer thickness, whichever is smaller [21,69]. For small Knudsen numbers, the solutions to the half-space problem discussed in Secs. 2.3, 3.1, and 4 give accurate jump conditions for practical evaporation/condensation scenarios in the moderately strong and strong regimes, and often in the weak mass transfer regime as well.

We note that for weak mass transfer ($|\Delta p^*| \ll 1$), conduction in the vapor phase may supply/remove the necessary heat for phase change [21,69]. In such cases, the half-space approximation for the Knudsen layer may be inaccurate as the external gradients become significant. Kogan [69] provided the following expressions for this scenario:

$$\rho_K u_K = \frac{\hat{\sigma}}{1 - 0.535\hat{\sigma}} \left(\frac{\rho_e - \rho_K}{\sqrt{2\pi/RT_L}} - 0.154 \frac{k}{R} \frac{\partial \ln T(0)}{\partial x} \right) \quad (18)$$

$$T_K^* = 1 - 0.44 \frac{u_K}{\sqrt{2RT_L}} + \frac{k}{p_K \sqrt{2RT_L}} \frac{\partial T(0)}{\partial x} \quad (19)$$

where k is the thermal conductivity of the vapor and $T(0)$ is the external (Navier–Stokes) solution evaluated at the Knudsen layer
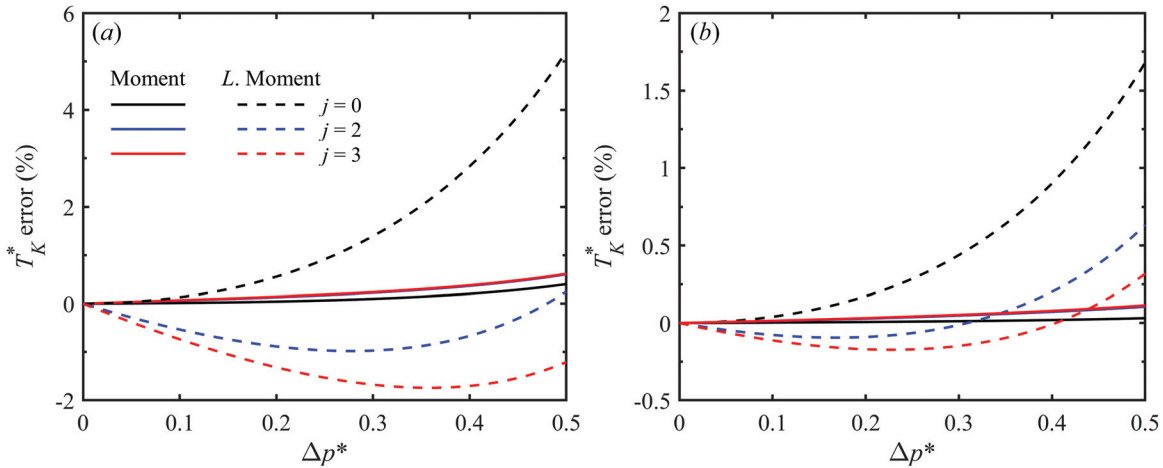
Fig. 8 Temperature ratio accuracies of the moment method (solid lines) and linearized moment method (dashed lines) for evaporation and (*a*) $\hat{\sigma} = 1$ or (*b*) $\hat{\sigma} = 0.25$. The black, blue, and red lines correspond to monatomic, polyatomic linear, and polyatomic nonlinear species, respectively. The moment method with Cercignani's accounting for rotational degrees-of-freedom is accurate within 0.6% for complete accommodation over this range (the *j* = 2 and *j* = 3 curves superimpose). For complete accommodation, the linearized moment method is within 1% deviation for $0 \leq \Delta p^* \leq 0.25$ for *j* = 0 and *j* = 2, but only achieves this level of accuracy in the range $0 \leq \Delta p^* \leq 0.14$ for *j* = 3. The relative errors for $\hat{\sigma} = 0.25$ are smaller for both approximations, suggesting that the temperature ratio prediction error decreases with decreasing $\hat{\sigma}$ like the flux prediction error.

boundary. When heat supply/removal occurs in the liquid or via radiation, the mass transfer rates can be stronger, and it has been shown that the half-space assumption for the Knudsen layer is valid since the external gradients become negligible [21,69]. Equations (18) and (19) converge to the half-space solutions under the condition $|\Delta p^*| \ll 1$, provided the external temperature gradient is small. Here, we focus on connecting the half-space approaches to the vapor flow.

The Schrage expressions provide a mass flux boundary condition at the liquid–vapor interface that depends on the pressure ratio and the temperature ratio, that is, p_K/p_e and T_K/T_L, consistent with the Knudsen layer-aware kinetic theory analysis of net condensation (Sec. 2.3). However, the implementation of the boundary condition must be different for net evaporation, as the kinetic theory dictates that only the pressure ratio or temperature ratio can be prescribed to give the mass flux. Choosing to prescribe the pressure ratio, , for instance, a boundary condition must be imposed on both the mass flux and T_K. In this way, the temperature of the vapor at the boundary is still related to the other variables, despite not appearing in the mass flux expression. Alternatively, the temperature ratio could be prescribed in the boundary condition and p_K would then be output alongside the mass flux. We note that because evaporation is a one-parameter problem, the vapor stream at the Knudsen layer boundary is not required to be in a saturated state. That is to, say, given an input Δp^*, the temperature ratio could correspond to a saturated, superheated, or supersaturated state, depending on the saturation curve of the fluid (Ytrehus [21] discusses this fact at greater length).

We remark here that when dealing with the classic case of condensation from a saturated vapor reservoir, p_K^* is often considered to be the pressure of the saturated vapor, but Eq. (17) does not guarantee that $T_K = T_{sat}(p_K)$. Therefore, the saturated condition occurs further upstream in the continuum region. This feature is not unique to the linear approximation of condensation; the same result is seen when coupling the fully nonlinear moment method to the Navier–Stokes description of the continuum region [21]. Depending on the fluid, it is even possible for an inverted temperature gradient to exist in the continuum region (with the vapor hotter closer to the liquid); this phenomenon is discussed in greater detail by Ytrehus [21] and Cercignani [38].

The final point we will comment on regarding the external continuum flow is that engineered systems commonly have a flow with a nonzero velocity component tangential to the liquid–vapor interface. The tangential velocity inside the Knudsen layer must be zero in the case of evaporation but not in the case of condensation [21,70,71]. However, the shear flow has little effect on the normal component of the condensing flow in the Knudsen layer unless the tangential Mach number ($M_{\tau K}$) is greater than 3 [21,71]. Thus, the effect of tangential flow on the Knudsen layer solution for condensation can safely be ignored when $M_{\tau K} \ll 1$.

Many more interesting aspects of evaporating and condensing flows have been studied by the kinetic theory community. We recommend Ytrehus' very thorough treatment of the half-space problem [21] (which includes a worked example for implementing Eqs. (16) and (17) in CFD), Kogan's review [69], Cercignani's textbook [38], Sone's textbook [15], and Frezzotti and Barbante's recent review [28]. These texts offer a plethora of information on the subject and point to many other enlightening publications.

5.2 On Temperature Ratio Estimation. Regarding the implementations we have discussed, the moment method correctly requires both p_K^* and T_K^* to compute J^* for condensation, while needing only one input to determine the other two quantities for evaporation. It is important to consider that small errors in calculating T_K^* for evaporation can often result in large discrepancies in the temperature difference $T_L - T_K$ because T_K^* is a ratio of absolute temperatures. For example, a 1% error in T_K^* at low fluxes and $T_L = 300$ K produces an error of ~ 3 K in $T_L - T_K$. The effect of internal degrees-of-freedom must also be considered: although we demonstrated in Sec. 3.5 that the flux is mostly insensitive to *j*, Frezzotti [43] pointed out that the same is not true of the temperature ratio. In comparison to the Holway model (with complete accommodation), the moment method predicts T_K^* for evaporation with at most 0.6% relative error (Fig. 8(*a*), the error would be significantly worse if not using Cercignani's method to account for internal degrees-of-freedom). The linearized moment method should be used cautiously when an accurate calculation of the temperature difference is required: its temperature ratio error exceeds 1% for $\Delta p^* > 0.25$ for *j* = 0 and *j* = 2, and for *j* = 3 it exceeds 1% when $\Delta p^* > 0.14$. As only the value of *j* affects the $T_K^*(p_K^*)$ relation for evaporation, Fig. 8(*a*) can be used to determine the T_K^* accuracy of these two methods for complete accommodation of any fluid in evaporation conditions up to $\Delta p^* = 0.5$. Both models see a reduced error for $\hat{\sigma} = 0.25$ (Fig. 8(*b*)), suggesting that the temperature ratio prediction error decreases with
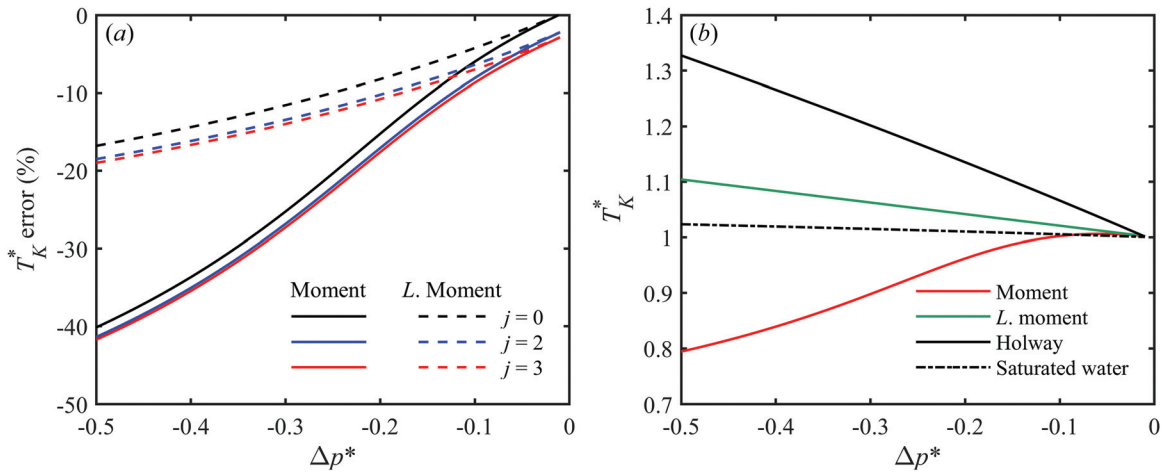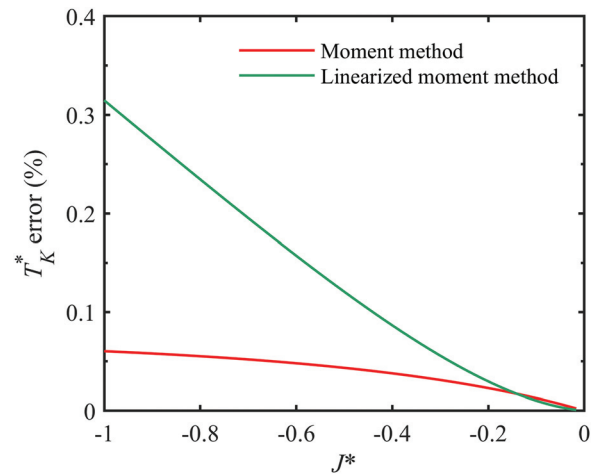
Fig. 9 (*a*) Temperature ratio accuracies of the moment method (solid lines) and linearized moment method (dashed lines) for condensation and $\hat{\sigma} = 1$. The black, blue, and red lines correspond to monatomic, polyatomic linear, and polyatomic nonlinear species, respectively. Both methods are significantly less accurate for condensation than evaporation, and the addition of internal degrees-of-freedom notably degrades their accuracy. (*b*) Temperature ratios corresponding to the monatomic data in (*a*). The dashed-dotted line represents the saturation curve of water at $T_L = 25\,°C$.

decreasing $\hat{\sigma}$ in the same manner as the flux prediction error. The temperature ratio error (and flux error) of these models for arbitrary values of $\hat{\sigma}$ can be directly calculated from the evaporation datasets we have provided (see Appendix F) by transforming the pressure ratio using Eq. (13) and comparing the transformed data to Eq. (16) and the moment method.

To quantify the temperature ratio prediction accuracy of the moment method for net condensation, we computed the temperature ratio predicted by the Holway model as a function of dimensionless driving pressure at the dimensionless flux given by the linearized moment method, i.e., $T_K^*(\Delta p^*, J_{\text{Eq. (16)}}^*(\Delta p^*))$. We assessed the accuracy of the moment method and linearized moment method by comparing $T_K^*(\Delta p^*, J_{\text{Eq. (16)}}^*(\Delta p^*))$ to $T_{K,\text{Moment}}^*(\Delta p^*, J_{\text{Eq. (16)}}^*(\Delta p^*))$ and $T_{K,\text{Eq. (17)}}^*(\Delta p^*)$, respectively, where the former is the temperature ratio predicted by the moment method at the dimensionless flux calculated by Eq. (16). These evaluations are shown in Fig. 9(*a*), where we find that the moment methods are much less accurate at temperature ratio prediction for condensation than evaporation. Further, we observe that these monatomic-specific models become more inaccurate when used to model species with two and three internal degrees-of-freedom.

However, one would expect from our findings in Sec. 3.5 that since the flux is weakly dependent on the temperature ratio, the temperature ratio ought to be strongly dependent on the flux if Δp^* and J^* are taken as the free parameters for condensation. Thus, the results of Fig. 9(*a*) should be highly specific to the condition $J^* = J_{\text{Eq.(16)}}^*(\Delta p^*)$. As shown in Fig. 9(*b*), this condition leads to large temperature ratios when the driving force for condensation is large. Comparing the temperature ratio calculated by the Holway model (solid black line in Fig. 9(*b*)) to the saturation curve of water at $T_L = 25\,°C$ (dashed-dotted black line in Fig. 9(*b*)), it is apparent that these conditions typically correspond to heavily superheated vapor. Further, we caution that the moment method can be more unreliable for temperature ratio prediction at high condensation fluxes than indicated in Fig. 9(*a*), see Appendix E3.

Another calculation of interest is to find the vapor saturation state needed to produce a certain condensing flux on a liquid at T_L. In contrast to the case demonstrated in Fig. 9, both Δp^* and T_K^* are adjustable parameters to match the flux, but are subject to the constraint $T_K^* = T_{\text{sat}}^*(\Delta p^*; T_L)$. We quantified the accuracy of the moment method and Eq. (16) for determining these saturated vapor states by comparing the predicted temperature ratios to that

Fig. 10 Temperature ratio errors of the moment method and its linearization for condensation of saturated water vapor at $T_L = 25\,°C$ and $\hat{\sigma} = 1$. Much greater accuracy is achieved when the saturated state $(\Delta p^*, T_{\text{sat}}^*(\Delta p^*))$ is the free parameter for matching the flux than when T_K^* is the sole free parameter for a fixed Δp^* and J^* (the results of Fig. 9(*a*)).

of the Holway model. We performed this analysis for saturated water vapor with $T_L = 25\,°C$ and $\hat{\sigma} = 1$ (Fig. 10). For the linearized moment method, we solved Eq. (16) for Δp^* and selected the temperature ratio from the saturation curve (using Eq. (17) results in a higher error and a nonsaturated state for the water vapor). In this scenario, the moment method and linearized moment method achieve less than 0.1% and 0.5% temperature prediction error, respectively.

6 Conclusions and Recommendations

The Schrage equations for evaporation or condensation rates of pure fluids have long been understood to satisfy neither momentum nor energy conservation at the liquid–vapor interface. We have quantified the inaccuracy of the Schrage equations via comparison to numerical solutions of the Holway model, an extension of the BGK model to polyatomic gases. Our conclusions summarized below apply to the range of conditions $-0.5 \leq \Delta p^* \leq 0.5$,

covering the low to moderately high flux regimes that are typically encountered in thermofluid engineering. Our key findings are:

(1) The complete Schrage expression (Eq. (6)) overpredicts evaporation/condensation fluxes by ~15% in the case of perfect accommodation.
(2) The explicit Schrage equation (Eq. (7)) overpredicts evaporation fluxes by more than Eq. (6), yet is more accurate than Eq. (6) in predicting condensation fluxes.
(3) For polar fluids such as water where the accommodation coefficient is likely less than 0.5, the explicit Schrage equation is typically accurate within 10%. Its accuracy tends to be higher for smaller values of $\hat{\sigma}$, although its error does not asymptotically tend to zero as $\hat{\sigma} \to 0$.

As our numerical solver for the Holway model is rather computationally expensive, we also analyzed the accuracy of the moment method (Eqs. (E1)–(E3), (E8)–(E10)) and the linearization of this moment method (Eqs. (16) and (17)) described by Ytrehus [21] and Cercignani [38]. Our findings and recommendations are:

(4) The moment method is a highly accurate model for mass flux, providing less than 0.4% flux prediction error for evaporation and less than 4% for condensation of monatomic fluids with complete accommodation. The temperature prediction error of the moment method for evaporation is less than 0.6% for any number of rotational degrees of freedom.
(5) The linearized moment method (Eqs. (16) and (17)) is quite accurate in the low flux regime, achieving less than 5% flux prediction error in the range $-0.1 < \Delta p^* < 0.1$ for monatomic fluids with complete accommodation. These equations are comparable in complexity to the explicit Schrage equation, which overpredicts fluxes by 16%–25% in the same range. For low flux evaporation ($0 \leq \Delta p^* < 0.1$), Eq. (17) provides a temperature ratio prediction error of less than 0.75% for any number of rotational degrees of freedom. Further, Eq. (16) is more accurate than the explicit Schrage equation for any $\Delta p^* \gtrsim -0.3$. We recommend using Eqs. (16) and (17) instead of the explicit Schrage equation.
(6) While the flux prediction accuracies mentioned in conclusions (4) and (5) apply to monatomic fluids, little additional error arises in applying these methods to polyatomic gases: the moment method relative errors increase to 1% and 4.1% for evaporation and condensation, respectively. For water—and other polyatomic species with low accommodation coefficients—these methods are more accurate than the values stated in (4) and (5) because their accuracy improves as $\hat{\sigma}$ decreases.
(7) Neither the moment method nor its linearization provides high-accuracy predictions of the temperature ratio for net condensation. Both models are only accurate for monatomic species at low fluxes. More theoretical work is needed to address the lack of computationally inexpensive, high-accuracy models for condensation. However, both models accurately predict saturated vapor states when the saturation constraint is enforced.

As liquid–vapor phase change devices reach increasingly high heat fluxes, high-accuracy models of the interfacial kinetic resistance become essential to the calculation of transport rates. Here, we have evaluated a selection of models based on a comparison to theoretical results. However, the moderate to strong mass transfer regimes of kinetically limited evaporation and condensation are difficult to access experimentally; thus, there is little data available for experimental validation. More experiments pushing further into the kinetically limited regime would be useful for such validation and clarification of the accommodation coefficients of various fluids. To facilitate the adoption of higher-accuracy alternatives to the Schrage equation, we have: (a) provided select sets of numerical data from our Holway model calculations (see Appendix F and Supplemental Materials on the ASME Digital Collection); (b) fit our data to engineering equations (see Appendix G); and (c) provided code for moment method calculations of evaporation and condensation for arbitrary values of $\hat{\sigma}$.[2] These approaches, as well as Eqs. (16) and (17), are valid for modeling evaporation/condensation in systems with vanishingly small Knudsen numbers and a single species in the vapor phase.

Nomenclature

a = hard sphere diameter, m
$a(x)$ = scalar functions in Eq. (14)
B = arbitrary constant
C_J = convergence criterion for flux
C_R = convergence criterion for residuals
$C_1 - C_4, D_1 - D_4, K_1 - K_4$ = constants for engineering equations
d = characteristic length scale, m
d_1 = constant used in spatial grid definition
d_2 = constant used in spatial grid definition
f = velocity distribution function, kgs^3/m^6
f' = velocity distribution function for a polyatomic gas, s^3/m^6 J
F = reduced distribution function, s/m^4
$\hat{F}$ = reduced local equilibrium distribution function, s/m^4
F^- = integration factor
G = reduced distribution function, 1/m^2/s
$\hat{G}$ = reduced local equilibrium distribution function, 1/m^2/s
G^- = integration factor
H = reduced distribution function, J s/m^4
$\hat{H}$ = reduced local equilibrium distribution function, J s/m^4
H^- = integration factor
H_j^- = modified integration factor
$I(f,\hat{f})$ = binary collision integral
j = number of internal degrees of freedom
J = mass flux, kg/m^2/s
k = thermal conductivity, W/m/K
k_B = Boltzmann constant, J/K
Kn = Knudsen number
L = normalized length of domain
m = particle mass, kg
M = Mach number
n = number density of molecules having rotational energy ϵ, 1/m^3/J
N = number density, 1/m^3
N_e' = modified number density defined by Eq. (B17), 1/m^3
p = pressure, Pa
Q = calculated quantity
R = specific gas constant, J/kg/K
S = speed ratio
t = time, s
T = temperature, K
$\boldsymbol{u}$ = net velocity vector, m/s
$\boldsymbol{x}$ = cartesian coordinate, m

---

[2]https://github.com/gvaartst/Moment-Method-for-Evaporation-Condensation

$\hat{x} =$ unit vector normal to the liquid/vapor interface directed toward the vapor phase
$\bar{z} =$ fraction of inelastic collisions

Greek Symbols

$\alpha^- =$ free parameter of the moment method for net condensation
$\beta^- =$ free parameter of the moment method
$\gamma =$ ratio of specific heats
$\Gamma =$ Schrage's correction factor
$\Gamma' =$ Schrage's correction factor, linearized
$\bar{\Gamma} =$ Gamma function
$\Delta p^* =$ dimensionless driving pressure
$\epsilon =$ rotational energy, J
$\eta =$ proportionality constant between dimensionless temperature and pressure jumps
$\lambda =$ mean free path, m
$\mu =$ kinematic viscosity, Pa s
$\nu =$ collision frequency, 1/s
$\xi =$ molecular velocity space coordinate
$\rho =$ density, kg/m^3
$\hat{\sigma} =$ accommodation coefficient
$\hat{\sigma}_c =$ condensation coefficient
$\hat{\sigma}_e =$ evaporation coefficient
$\Phi =$ local equilibrium distribution function
$\chi =$ accommodation prefactor
$\omega =$ constant used in Eqs. (16) and (17)
$\omega' =$ constant used in Eq. (17)

Other Symbols

$\infty =$ infinity, far field

Subscripts

$c =$ characteristic
$e =$ equilibrium
el $=$ elastic
$H =$ Holway
hs $=$ hard sphere
$i =$ index
in $=$ inelastic
$J =$ flux
$k =$ index
$K =$ Knudsen
$L =$ liquid
$M =$ Maxwell–Boltzmann distribution
mod $=$ model
$r =$ rotational
$R =$ relative
sat $=$ saturation
$t =$ translational
tot $=$ total
$v =$ vapor
$x =$ vector component
$\tau =$ tangential
$4 =$ fourth mode

Superscripts

$(i) =$ Cartesian grid point
$(k) =$ velocity grid point
$* =$ normalized variable
$+ = \xi_x > 0$ portion of a distribution function or flux
$- = \xi_x < 0$ portion of a distribution function or flux

Abbreviations

BGK $=$ Bhatnagar, Gross, and Krook
BTE $=$ Boltzmann transport equation
DSMC $=$ direct simulation Monte Carlo

Appendix A: The Velocity Distribution Function, Thermodynamic State, and Flow Velocity

The velocity distribution function describes the local thermodynamic state and macroscopic flow velocity of gas via the relations

$$\rho = \int f d\xi_x d\xi_y d\xi_z \qquad \text{(A1)}$$

$$RT = \frac{1}{3\rho} \int |\boldsymbol{\xi} - \boldsymbol{u}|^2 f d\xi_x d\xi_y d\xi_z \qquad \text{(A2)}$$

$$u_x = \frac{1}{\rho} \int \xi_x f d\xi_x d\xi_y d\xi_z \qquad \text{(A3)}$$

We note that there are alternative definitions of f used in the literature that slightly change Eqs. (A1)–(A3), but in no way alter the fundamental description of gas kinetics. For example, f is often defined as the number of molecules per unit volume in a differential volume of the velocity space. In this case, ρ is replaced by the number density N in Eqs. (A1)–(A3) and $\rho = mN$, where m is the mass of one molecule of the gas species.

Appendix B: Holway's Model and Numerical Solution

B.1 Model Formulation. Following Frezzotti's approach [43], the local equilibrium distributions in the collision operator of Holway's model (Eq. (11)) are

$$\Phi_{el}(\boldsymbol{\xi}, \epsilon) = \frac{n(\epsilon|\boldsymbol{x}, t)}{[2\pi RT_t(\boldsymbol{x}, t)]^{3/2}} \exp\left(-\frac{|\boldsymbol{\xi} - \boldsymbol{u}(\boldsymbol{x}, t)|^2}{2RT_t(\boldsymbol{x}, t)}\right) \qquad \text{(B1)}$$

$$\Phi_{in}(\boldsymbol{\xi}, \epsilon) = \frac{N(\boldsymbol{x}, t)}{[2\pi RT(\boldsymbol{x}, t)]^{3/2}} \exp\left(-\frac{|\boldsymbol{\xi} - \boldsymbol{u}(\boldsymbol{x}, t)|^2}{2RT(\boldsymbol{x}, t)}\right)$$
$$\frac{\epsilon^{j/2-1}}{\bar{\Gamma}(j/2)[k_B T(\boldsymbol{x}, t)]^{j/2}} \exp\left(-\frac{\epsilon}{k_B T(\boldsymbol{x}, t)}\right) \qquad \text{(B2)}$$

where n is the number density of molecules with rotational energy ϵ, $\bar{\Gamma}$ is the complete Gamma function, and k_B is the Boltzmann constant. Frezzotti calculated the collision frequencies from the shear viscosity of a hard sphere gas (μ_{hs}) as

$$\nu_{el}(N, T_t) = (1 - \bar{z})\nu_{tot}(N, T_t) \qquad \text{(B3)}$$

$$\nu_{in}(N, T_t) = \bar{z}\nu_{tot}(N, T_t) \qquad \text{(B4)}$$

$$\nu_{tot}(N, T_t) = \frac{Nk_B T_t}{\mu_{hs}(T_t)} \qquad \text{(B5)}$$

$$\mu_{hs} = \frac{5}{16} \frac{\sqrt{\pi m k_B T_t}}{\pi a^2} \qquad \text{(B6)}$$

where $\bar{z}$ is the fraction of inelastic collisions and a is the hard sphere diameter. Here we select $\bar{z} = 0.3$ (consistent with Refs. [43] and [55]), noting that Frezzotti [43] observed that changing $\bar{z}$ from 0.3 to 1 affects the structure of the Knudsen layer but not p_K^*, T_K^*, and $u_K/\sqrt{2RT_L}$. For the half-space problem, the numerical solution Eq. (10) with Eq. (11) as the collision term can be simplified to a system of equations that only requires velocity discretization in one dimension. This can be achieved following Chu's transformation [72] to define the reduced distribution functions

$$\begin{pmatrix} F(\xi_x|x,t) \\ G(\xi_x|x,t) \\ H(\xi_x|x,t) \end{pmatrix} = \int \begin{pmatrix} 1 \\ \xi_y^2 + \xi_z^2 \\ \epsilon \end{pmatrix} f'(\xi,\epsilon|x,t,)d\xi_y d\xi_z d\epsilon \quad \text{(B7)}$$

where we use f' to denote the number density in a differential volume of the molecular velocity and rotational energy space. The governing system of equations in the steady-state is then

$$\xi_x \frac{\partial}{\partial x} \begin{pmatrix} F \\ G \\ H \end{pmatrix} = \nu_{\mathrm{el}} \begin{pmatrix} \hat{F}_{\mathrm{el}} - F \\ \hat{G}_{\mathrm{el}} - G \\ \hat{H}_{\mathrm{el}} - H \end{pmatrix} + \nu_{\mathrm{in}} \begin{pmatrix} \hat{F}_{\mathrm{in}} - F \\ \hat{G}_{\mathrm{in}} - G \\ \hat{H}_{\mathrm{in}} - H \end{pmatrix} \quad \text{(B8)}$$

The reduced local equilibrium distributions are

$$\begin{pmatrix} \hat{F}_{\mathrm{el}}(\xi_x|x,t) \\ \hat{G}_{\mathrm{el}}(\xi_x|x,t) \\ \hat{H}_{\mathrm{el}}(\xi_x|x,t) \end{pmatrix} = \begin{pmatrix} 1 \\ 2RT_t(x,t) \\ \frac{jk_B T_r(x,t)}{2} \end{pmatrix} \frac{N(x,t)}{\sqrt{2\pi RT_t}} \exp\left(-\frac{(\xi_x - u_x)^2}{2RT_t}\right)$$
$$\text{(B9)}$$

$$\begin{pmatrix} \hat{F}_{\mathrm{in}}(\xi_x|x,t) \\ \hat{G}_{\mathrm{in}}(\xi_x|x,t) \\ \hat{H}_{\mathrm{in}}(\xi_x|x,t) \end{pmatrix} = \begin{pmatrix} 1 \\ 2RT(x,t) \\ \frac{jk_B T(x,t)}{2} \end{pmatrix} \frac{N(x,t)}{\sqrt{2\pi RT}} \exp\left(-\frac{(\xi_x - u_x)^2}{2RT}\right)$$
$$\text{(B10)}$$

where T_r is the rotational temperature. The thermodynamic variables and flow velocity can be computed from F, G, and H as

$$N(x,t) = \int F d\xi_x \quad \text{(B11)}$$

$$T_t(x,t) = \frac{1}{3RN(x,t)} \left(\int (\xi_x - u_x)^2 F d\xi_x + \int G d\xi_x \right) \quad \text{(B12)}$$

$$T_r(x,t) = \frac{2}{jk_B N(x,t)} \int H d\xi_x \quad \text{(B13)}$$

$$T(x,t) = \frac{3T_t(x,t) + jT_r(x,t)}{3+j} \quad \text{(B14)}$$

$$u_x(x,t) = \frac{1}{N(x,t)} \int \xi_x F d\xi_x \quad \text{(B15)}$$

The boundary conditions at the liquid–vapor interface $(x=0)$ are

$$\begin{pmatrix} F(\xi_x|0,t) \\ G(\xi_x|0,t) \\ H(\xi_x|0,t) \end{pmatrix} = \begin{pmatrix} 1 \\ 2RT_L \\ \frac{jk_B T_L}{2} \end{pmatrix} \frac{N'_e}{\sqrt{2\pi RT_L}} \exp\left(-\frac{\xi_x^2}{2RT_L}\right), \quad \xi_x > 0$$
$$\text{(B16)}$$

where N'_e is the number density at the wall accounting for evaporating and diffusely reflected molecules

$$N'_e = \hat{\sigma} N_e + (1 - \hat{\sigma})|J_L^-|\sqrt{\frac{2\pi}{RT_L}} \quad \text{(B17)}$$

$$J_L^- = \int_{\xi_x < 0} \xi_x F(\xi_x|0,t) d\xi_x \quad \text{(B18)}$$

and N_e is the equilibrium number density of the vapor at T_L. Finally, the far field boundary conditions are

$$\lim_{x \to \infty} \begin{pmatrix} F(\xi_x|x,t) \\ G(\xi_x|x,t) \\ H(\xi_x|x,t) \end{pmatrix} = \begin{pmatrix} 1 \\ 2RT_K \\ \frac{jk_B T_K}{2} \end{pmatrix} \frac{N_K}{\sqrt{2\pi RT_K}} \exp\left(-\frac{(\xi_x - u_K)^2}{2RT_K}\right),$$
$$\xi_x < 0 \qquad \text{(B19)}$$

Here we have again used the subscript "K" for macroscopic variables at the Knudsen layer boundary, a state which is approached at $x \to \infty$ of the system Eq. (B8).

B.2 Numerical Method. We solved Eq. (B8) via the finite difference method with a second-order upwind scheme, similar to that described by Kazuo et al. [51]. We first normalized the Holway model system by converting to the scaled variables $N^* = N/N_e$, $T^* = T/T_L$, $\xi_x^* = \xi_x/\sqrt{2RT_L}$, $\epsilon^* = \epsilon/k_B T_L$, and $x^* = x/\lambda_{hs}$, where λ_{hs} is the hard-sphere mean free path

$$\lambda_{hs} = \frac{1}{\sqrt{2\pi N_e a^2}} \quad \text{(B20)}$$

We discretized the ξ_x^* space into equally spaced cells with a maximum spacing of $0.02/\sqrt{2}$ (or $0.02\sqrt{RT_L}$ in dimensional velocity space). The dimensionless versions of Eqs. (B11)–(B13), (B15) were evaluated using trapezoidal integration over the dimensionless velocity space, which we chose to span $-8/\sqrt{2} \le \xi_x^* \le 8/\sqrt{2}$. The x^* space was discretized on a grid with variable spacing such that the grid spacing was smaller near $x^* = 0$, where spatial gradients are highest. Using i and k to denote points in the cartesian/ velocity space (i.e., $(x^{*(i)}, \xi_x^{*(k)})$), we defined the cartesian grid as

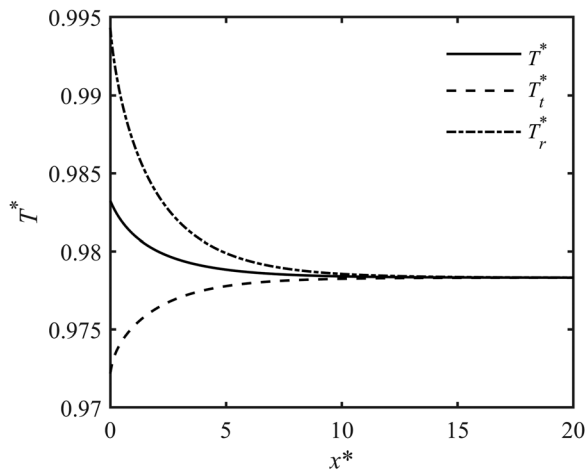$$x^{*(i)} = d_1 i + (1/4)(d_2 - d_1)(i^4/N_x^3), \quad (i = 0, 1, \dots N_x) \quad \text{(B21)}$$

with spacing

$$\Delta x^{*(i)} = d_1 + (d_2 - d_1)(i^3/N_x^3), \quad (i = 0, 1, \dots N_x) \quad \text{(B22)}$$

where $d_1 = 0.002$, $d_2 = 4L/N_x - 3d_1$, and L is the normalized length of the domain (i.e., the dimensionless domain spans $0 \le x^* \le L$). Both N_x and L were varied among the many calculations we made to ensure that the gradients and Knudsen layer thicknesses unique to each set of conditions were accurately resolved. This grid definition is similar to that of Kazuo et al. [51], and we used their second-order upwind scheme

$$\frac{\partial}{\partial x^*} \phi_{i,k} = \begin{cases} -\left(3/2\phi_{i,k} - 2\phi_{i+1,k} + 1/2\phi_{i+2,k}\right)/\Delta x^{*(i)}, & 0 \le i \le N_x, \quad k < 0 \\ \left(3/2\phi_{i,k} - 2\phi_{i-1,k} + 1/2\phi_{i-2,k}\right)/\Delta x^{*(i)}, & 2 \le i \le N_x, \\ (\phi_{1,k} - \phi_{0,k})/\Delta x^{*(1)}, & i = 1, \end{cases} \quad k \ge 0 \quad \text{(B23)}$$
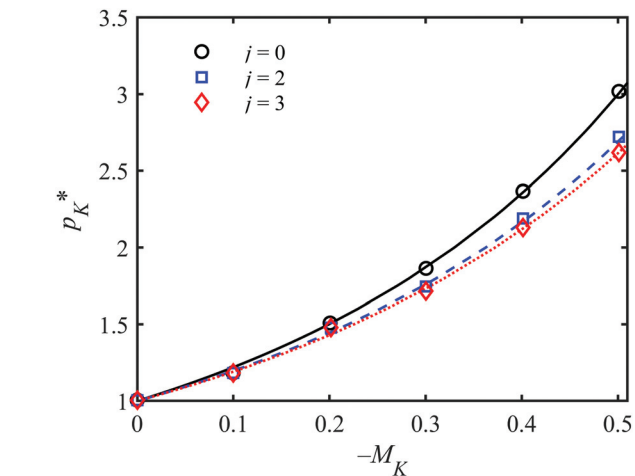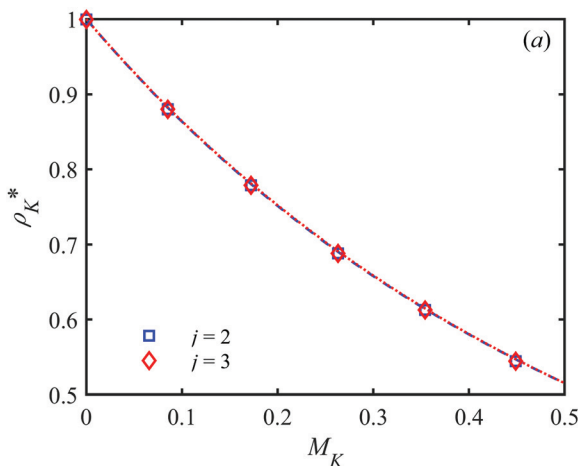
Fig. 11 Dimensionless total, translational, and rotational temperature relaxation in the Knudsen layer for $j = 3$ and $M_K = 0.1$
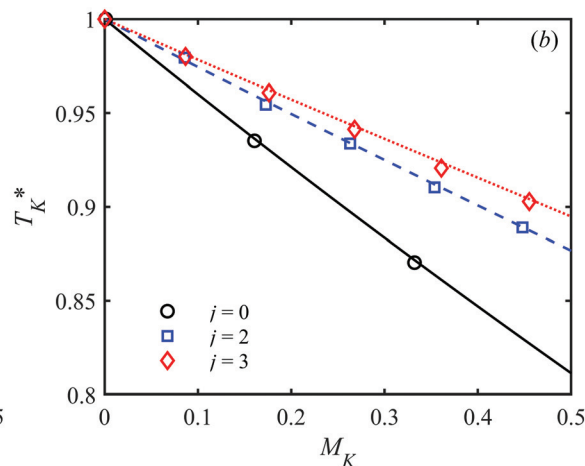
Fig. 13 Validation of our implementation of the Holway model (lines) against Frezzotti and Ytrehus' [55] DSMC calculations (symbols) for condensation with $T_K^* = 1$. Our implementation accurately reproduces the relation between pressure ratio and far-field Mach number for 0, 2, and 3 rotational degrees-of-freedom. Our Holway model results are shown as a solid black line for $j = 0$, a dashed blue line for $j = 2$, and a dotted red line for $j = 3$.

where $\xi_x^{(0)} = 0$ (thus $k < 0$ are the negative velocities) and $\phi_{i,k}$ is the dimensionless version of F, G, or H at point $(x^{*(i)}, \xi_x^{*(k)})$. To enforce the Neumann boundary condition for $k < 0$ at $x^* = L$, we set $\phi_{N_x,k} = \phi_{N_x+1,k} = \phi_{N_x+2,k}$. We note that there is no need to define the gradient at $i = 0$ for $k \geq 0$ due to the Dirichlet boundary condition there. We used a quasi-Newton method to solve the discretized system of equations iteratively until the maximum residual of the dimensionless, discretized version of Eq. (B8) was $C_R < 10^{-10}$ and the relative change of the dimensionless mass flux with respect to the previous step was $C_J < 10^{-13}$. These strict convergence criteria were met in all calculations besides the lowest Mach number condensation cases, where such standards were computationally challenging to meet since the Knudsen layer is very thick. Even these cases still converged well, typically meeting $C_R < 10^{-7}$ and $C_J < 10^{-10}$.

B.3 Typical Numerical Results. We illustrate some typical numerical results in Fig. 11, where we have solved the Holway model system for a species with $j = 3$ evaporating at $M_K = 0.1$. The translational and rotational temperatures are perturbed at the liquid–vapor interface ($x^* = 0$) but relax to the equilibrium value $T^* = 0.9783$ within tens of mean free paths (these calculations were made with a domain of $L = 74$, we truncated the

plot to highlight the region of strong nonequilibrium). The maximum deviation of the dimensionless mass flux across the domain is less than 0.0002% for this example, demonstrating the accuracy of this numerical method.

B.4 Validation. We have validated our implementation of Holway's model equation by comparison to the DSMC data for evaporation and condensation from Frezzotti [43] and Frezzotti and Ytrehus [55], respectively. Figures 12 and 13 demonstrate the high degree of fidelity with which our finite difference implementation reproduces the relationships among the macroscopic flow parameters of the reference DSMC data. The authors of those original works also noted that the Holway model accurately reproduced their DSMC calculations [43,55].

As further validation of our numerical results, we compare our mass flux calculations to the experimental data of Lu et al. [58] for evaporation of water (Fig. 14). We used $\hat{\sigma} = 0.31$, the accommodation coefficient found by those authors upon fitting DSMC calculations to their experimental data. The good agreement of our

Fig. 12 Validation of our implementation of the Holway model (lines) against Frezzotti's [43] DSMC calculations (symbols) for evaporation. Our implementation accurately reproduces the relations of (a) the density ratio and (b) the temperature ratio to the far-field Mach number. Our Holway model results are shown as solid black lines for $j = 0$, dashed blue lines for $j = 2$, and dotted red lines for $j = 3$.
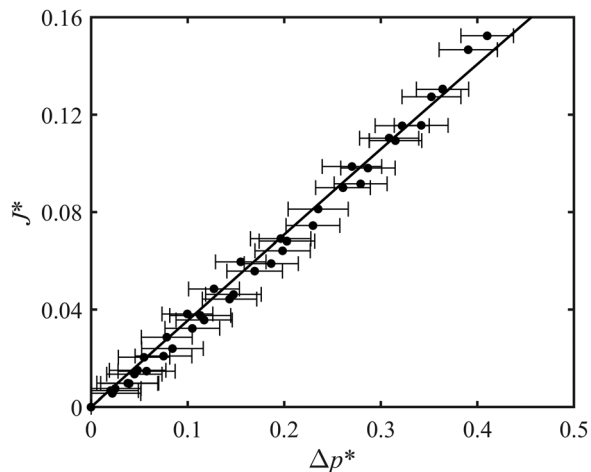
Fig. 14 Validation of our implementation of the Holway model (solid line) against the experimental data of Lu et al. [58] (symbols) for evaporation of water. We used $\hat{\sigma} = 0.31$, the same accommodation coefficient those authors reported by fitting DSMC calculations to their experimental data.
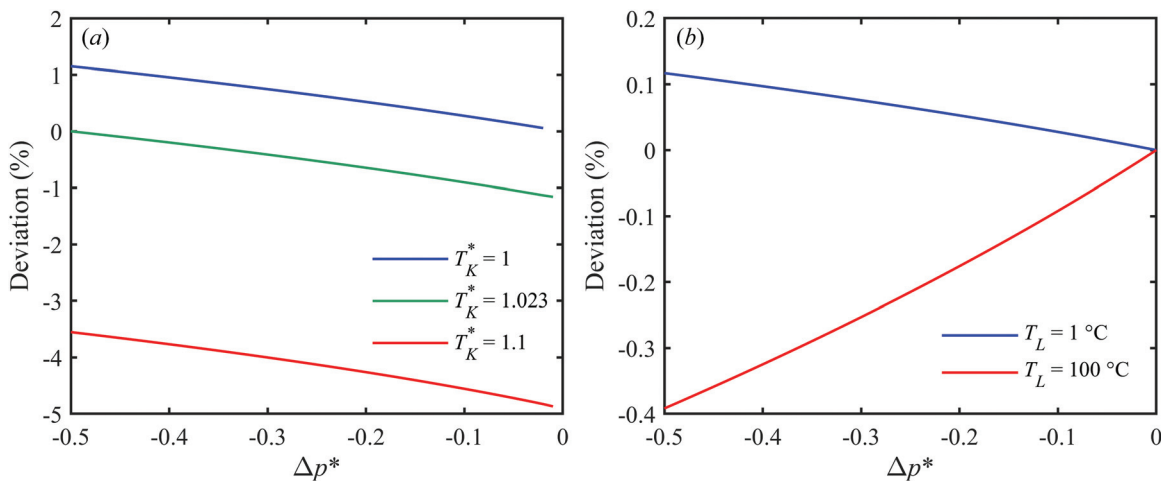
calculations with their experimental data and DSMC calculations is evidence that the Holway model sufficiently captures the collision dynamics of water molecules despite its relative simplicity.
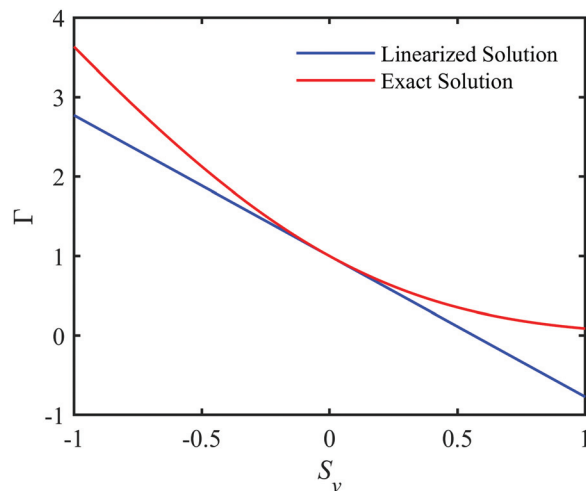
Appendix C: More on Schrage's Equation

Including the accommodation effect, Eq. (E4a) becomes

$$\hat{\sigma} \int_{\xi_x > 0} \xi_x f_L^+ d\boldsymbol{\xi} + \int_{\xi_x < 0} \xi_x f_L^- d\boldsymbol{\xi} - (1 - \hat{\sigma}) \int_{\xi_x < 0} \xi_x f_L^- d\boldsymbol{\xi} = \rho_v u_v$$

(C1)

Substituting Eq. (5) into Eq. (C1) and performing the integrations on the left-hand side introduces the correction factor Γ (see Eq. (6)) into the framework of the Hertz-Knudsen equation, thus accounting for the bulk motion of the vapor. Under this framework, Γ essentially scales the magnitude of the condensing stream. The linearization of Γ proposed by Nabavian and Bromley [23] (Γ'), always produces a smaller correction factor than the exact solution (Fig. 15).
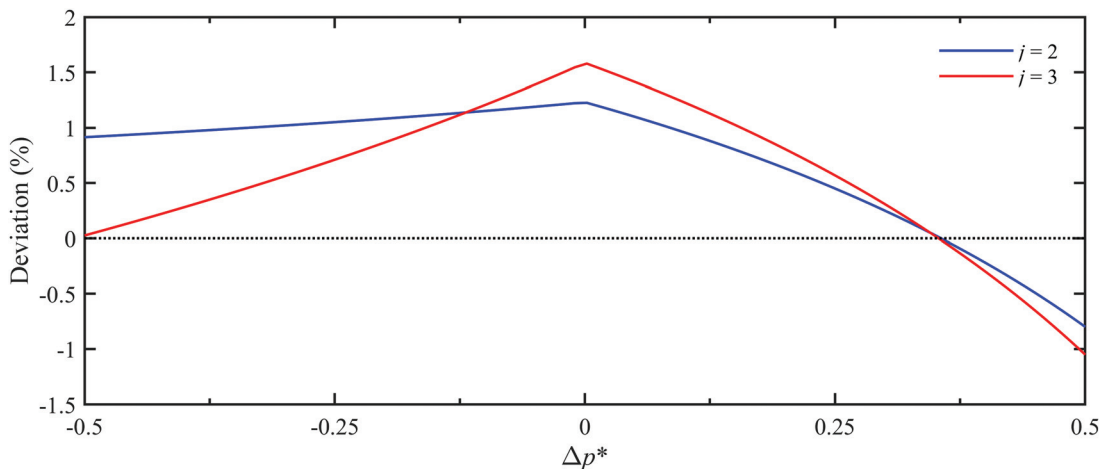

Fig. 15 The linearized solution to Schrage's correction factor (referred to as Γ' in the text) is always smaller than the exact expression for the same speed ratio. As a result, Eq. (7) always underestimates the magnitude of the condensing stream compared to Eq. (6).

Appendix D: Flux Dependence on Secondary Variables

We observed that the condensation flux, $J^*(\Delta p^*, T_K^*)$, is primarily a function of Δp^* when T_K is restricted to be reasonably near $T_{sat}(p_K)$. To demonstrate this, we show the relative error of choosing a fixed value of T_K^* (while varying Δp^*) to calculate J^* for condensation of water from saturated vapor to $T_L = 25\,^\circ\text{C}$ (Fig. 16(a)). $T_K^* = 1 = T_{sat}^*(\Delta p^* = 0)$ and $T_K^* = 1.023 = T_{sat}^*$ $(\Delta p = -0.5; T_L = 25\,^\circ\text{C})$ are the bounds of the saturation curve for $-0.5 < \Delta p^* < 0$ at this condition. The fluxes calculated in these two cases deviate by $\sim 1\%$ from $J^*(\Delta p^*, T_K^*|_{sat}; T_L = 25\,^\circ\text{C})$ at worst. As a fairly extreme state of superheated vapor, fixing $T_K^* = 1.1$ still reproduces the flux from the saturated state with less than 5% error. Varying the liquid temperature for condensation of saturated water vapor also has little impact on the dimensionless flux (Fig. 16(b)).

As reported by Frezzotti and Ytrehus [55], we observe that the dimensionless mass flux curves for species with different numbers of rotational degrees-of-freedom nearly collapse to one curve (Fig. 17).

Fig. 16 (a) Relative deviation of the condensation flux for fixed values of T_K^* compared to the relation for saturated water vapor at $T_L = 25\,^\circ\text{C}$. $T_K^* = 1.023$ corresponds to $T_{sat}^*(\Delta p_K^* = -0.5; T_L = 25\,^\circ\text{C})$; thus the blue and green curves bound the error of using one T_K^* from the saturation curve to estimate the condensation data of Fig. 1(a). (b) Relative deviation of $J^*(\Delta p^*, T_K^*|_{sat})$ for water at $T_L = 1\,^\circ\text{C}, 100\,^\circ\text{C}$ compared to $T_L = 25\,^\circ\text{C}$.

Fig. 17 Deviation of J^* for 2 or 3 internal degrees-of-freedom compared to a monatomic species (with $T_K^* = 1$ set for condensation). The dotted line is a guide to the eye for zero relative error.

Appendix E: Moment Method

E.1 Conservation Equations. The moment method extension to evaporation of polyatomic species (and complete accommodation) proposed by Cercignani [68] results in the following system of equations for mass, momentum, and energy conservation

$$\frac{\sqrt{T_K^*}}{p_K^*} - \beta^- F^- = 2\sqrt{\pi} S_K \qquad (E1)$$

$$\frac{1}{p_K^*} + \beta^- G^- = 4S_K^2 + 2 \qquad (E2)$$

$$\frac{1}{p_K^*}\frac{j+4}{4} - \beta^- H_j^- \sqrt{T_K^*} = \sqrt{\pi T_K^*} S_K\left(S_K^2 + \frac{5+j}{2}\right) \qquad (E3)$$

where $\beta^- = a_K^-(0)$ and

$$F^- = e^{-S_K^2} - \sqrt{\pi} S_K erfc(S_K) \qquad (E4)$$

$$G^- = \left(2S_K^2 + 1\right) erfc(S_K) - \frac{2}{\sqrt{\pi}}S_K e^{-S_K^2} \qquad (E5)$$

$$H^- = \frac{1}{2}\left(S_K^2 + 2\right)e^{-S_K^2} - \frac{\sqrt{\pi}}{2} S_K\left(S_K^2 + \frac{5}{2}\right) erfc(S_K) \qquad (E6)$$

$$H_j^- = H^- + \frac{j}{4}F^- \qquad (E7)$$

The system of Eqs. (E1)–(E3) is solved by specifying one of p_K^*, T_K^*, or S_K and solving for the other two parameters and β^-. We note that F^- is exactly Schrage's correction factor, Γ. In fact, Eq. (E1) is exactly Schrage's equation if one sets $\beta^- = 1$. For net condensation, the system of equations resulting from the substitution of Ytrehus' *ansatz* [47] into Eq. (4) is

$$\frac{\sqrt{T_K^*}}{p_K^*} - \beta^- F^- - \frac{p_4^*}{p_K^*}\sqrt{\frac{T_K^*}{T_4^*}}\alpha^- F_4^- = 2\sqrt{\pi} S_K \qquad (E8)$$

$$\frac{1}{p_K^*} + \beta^- G^- + \frac{p_4^*}{p_K^*}\alpha^- G_4^- = 4S_K^2 + 2 \qquad (E9)$$

$$\frac{1}{p_K^*} - \sqrt{T_K^*}\beta^- H^- - \frac{p_4^*}{p_K^*}\sqrt{T_4^*}\alpha^- H_4^- = \sqrt{\pi T_K^*} S_K\left(S_K^2 + \frac{5}{2}\right) \qquad (E10)$$

where $\alpha^- = a_4^-(0)$

$$p_4^* = \frac{1}{2}\left(1 - \frac{2}{3\pi}\right) \qquad (E11)$$

$$T_4^* = \left(1 - \frac{2}{3\pi}\right) \qquad (E12)$$

and F_4^-, G_4^-, and H_4^- are F^-, G^-, and H^- evaluated at $S_4 = 1/\sqrt{\pi - 2/3}$. The system of Eqs. (E8)–(E10) is solved by specifying two of p_K^*, T_K^*, or S_K and solving for the remaining parameter, β^-, and α^-. Ytrehus [21] and Cercignani [38] discuss the moment method in greater detail.[3] In the case of $\hat{\sigma} \neq 1$, all p_K^* terms in the conservation equations should be substituted with the $(p_K^*)_{\hat{\sigma}=1}$ expression that results from rearranging Eq. (13). We do not further discuss Shankar and Marble's [48] moment analysis here because it has not often been used by others, although it provides a similar result to the linearization of the moment method discussed here (Eq. (16)).

E.2 Effects of $\hat{\sigma}$ and j on Accuracy. As is the case with the Schrage equations, the moment method and its linearization gain flux prediction accuracy as the accommodation coefficient decreases (Fig. 18). Figure 19 compares the explicit Schrage equation, moment method, and linearized moment method to Holway model calculations for polyatomic ($j = 3$) fluids, where saturated water at $T_L = 25\,^\circ\text{C}$ is considered for the condensation regime. These results are similar to the comparison among models for monatomic fluids made in Fig. 7. The relative errors of the moment method for evaporation and condensation slightly increase to 1% and 4.1%, respectively. Recalling that the moment method for net condensation and the linearized moment method does not account for internal degrees-of-freedom, only the net evaporation moment method (and Holway model) calculations in Fig. 19 distinguish the fluid as polyatomic.

---

[3]Equations (8.3.13)–(8.3.15) of Cercignani's textbook [38], the dimensionless moment equations for condensation, contain a few typographical errors. The correct dimensionless expressions are listed here as Eqs. (E8)–(E10) and the correct dimensional expressions are given by Ytrehus (Eqs. (5.11a)–(5.11c) of Ref. [21]).
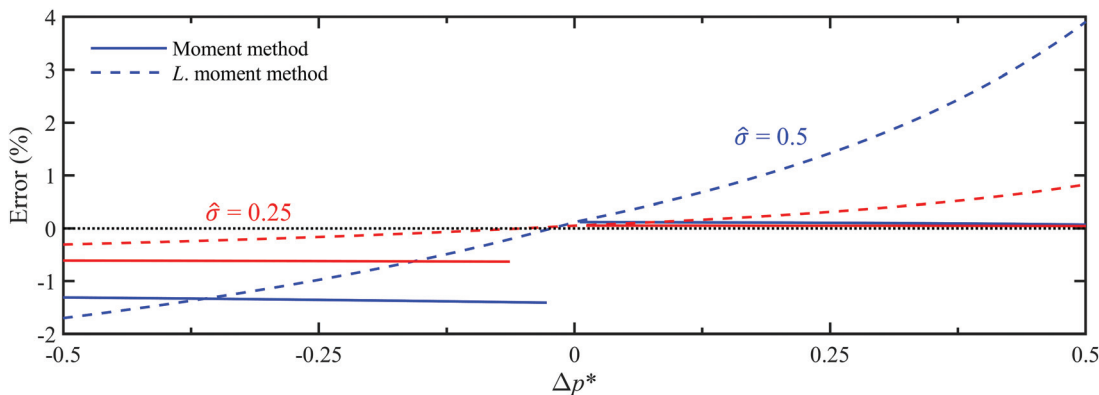
Fig. 18 Effect of the accommodation coefficient on flux prediction accuracy of the moment method and its linearization. As with the Schrage equations, the accuracy of both models improves as $\hat{\sigma}$ decreases. Here we considered a monatomic species with $T_K^* = 1$ fixed for net condensation. The dotted line is a guide to the eye for zero relative error.
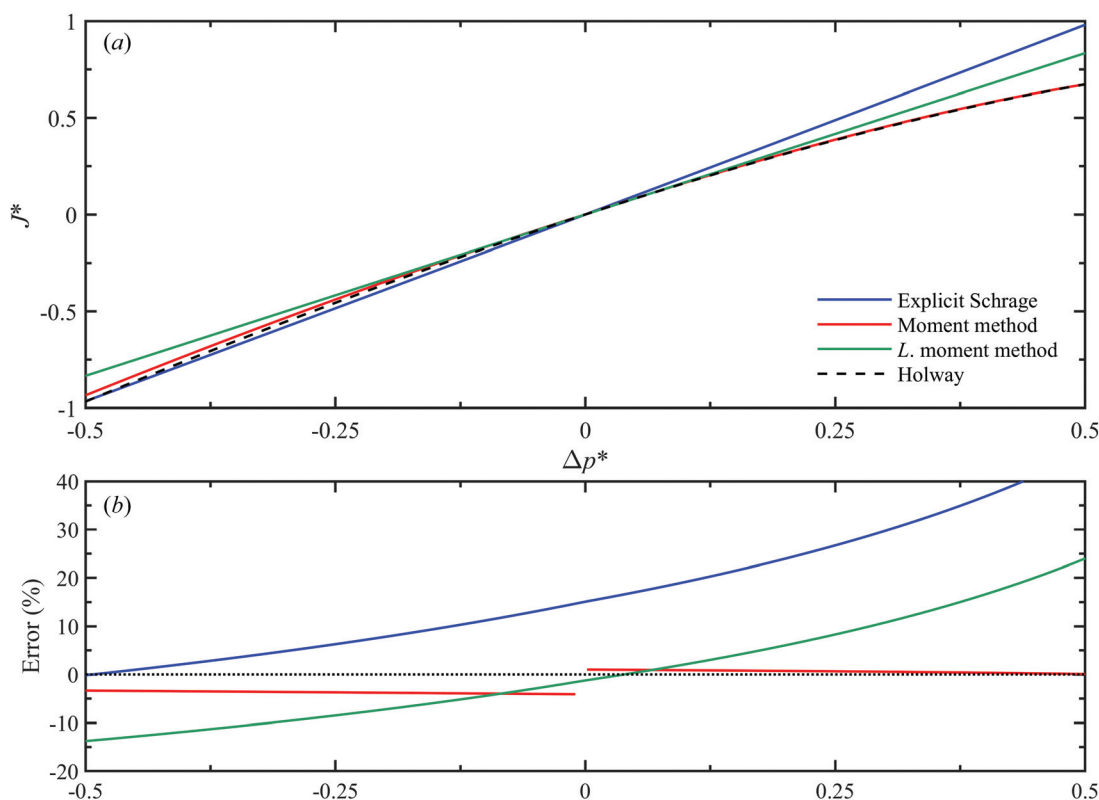
Fig. 19 Comparison of the explicit Schrage equation (Eq. (7)), moment method, and linearized moment method (Eq. (16), *L.* moment method) for polyatomic fluids (*j* = 3) with complete accommodation. For condensation, the temperature ratio corresponds to saturated water at $T_L = 25\,^\circ\text{C}$. The moment method deviates less than 1% and less than 4.1% from the Holway model for evaporation and condensation, respectively. The dotted line in (*b*) is a guide to the eye for zero relative error.

E.3 Note on Temperature Ratio Prediction for Condensation. We caution the reader that using the moment method described here for condensation to predict $T_K^*(\Delta p^*, J^*)$ may yield unreliable results, especially at higher fluxes. Defining a proportionality constant η as

$$\Delta p^* = \eta(1 - T_K^*) \qquad (E13)$$

Ytrehus [73] noted that the solution breaks down when

$$\eta > 1.79127 \text{ or } \eta < -4.08841 \qquad (E14)$$

but did not comment on whether the accommodation coefficient affects these critical values. Further, we found that the moment method calculations of dimensionless flux as a function of temperature ratio at certain fixed values of Δp^* do not have the same trend as the Holway model (see Fig. 20, where $\Delta p^* = -0.35$ is fixed). Two issues that may arise at conditions like these are: (a) the moment method could erroneously predict two different temperature ratios corresponding to the same Δp^* and J^*, especially if the bounds of Eq. (E14) are ignored; and (b) the moment method may give no solution for $T_K^*(\Delta p^*, J^*)$ (e.g., at higher fluxes in Fig. 20). We have not explored these issues extensively but have
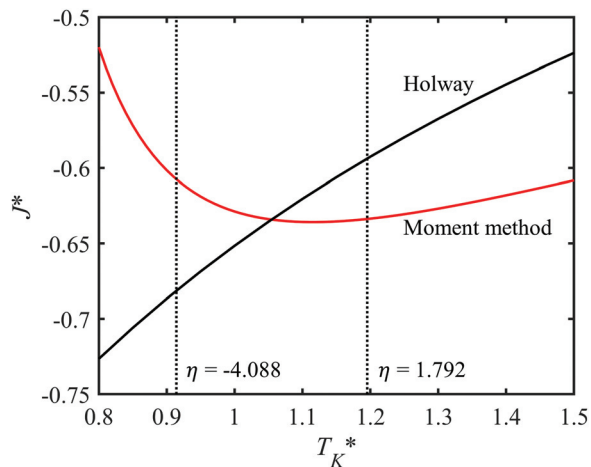
Fig. 20 Dimensionless flux as a function of temperature ratio holding $\Delta p^* = -0.35$ with complete accommodation. According to Ytrehus' analysis [73], the moment method for condensation is valid in the region between the vertical dotted lines. We note that if this region is ignored, the moment method could incorrectly provide two different T_K^* for the same Δp^* and J^*, e.g., at $\Delta p^* = -0.35$, $J^* = -0.625$. Another problem is that the moment method will give no solution for T_K^* at higher fluxes, e.g., at $\Delta p^* = -0.35$, $J^* = -0.7$.

noticed that they tend to occur at higher values of Δp^*. Accordingly, caution should be exercised when using this moment method to estimate $T_K^*(\Delta p^*, J^*)$ at higher fluxes.

Appendix F: Numerical Data

Spreadsheets of select sets of our numerical data are available for download from the Supplemental Materials on the ASME Digital Collection. There is one spreadsheet each for evaporation of species with $j = 0, 2, 3$, and complete accommodation. With these datasets, it is possible to model evaporation processes with $0 \leq \Delta p^* \leq 0.5$ for any value of $\hat{\sigma}$ by applying the transform Eq. (13) to the dataset. The final spreadsheet is for condensation of saturated vapor water at $T_L = 25\,^\circ\text{C}$. According to the analysis of 3.5, the relation between J^* and Δp^* from this dataset could be used to model condensation with different fluids/operating conditions without incurring much error.

Appendix G: Engineering Equations

We have fit engineering equations to our Holway model data of the form

$$J^* = \left(C_1\chi + C_2\chi^2\right)\left(C_3\Delta p^* + C_4\Delta p^{*2}\right) \quad \text{for} \quad \hat{\sigma} \leq 0.75 \quad \text{(G1)}$$

$$J^* = \left(D_1\chi + D_2\chi^2\right)\left(D_3\Delta p^* + D_4\Delta p^{*2}\right) \quad \text{for} \quad 0.75 < \hat{\sigma} \leq 1 \quad \text{(G2)}$$

$$T_K^* = 1 - \left(K_1\chi + K_2\chi^2\right)\left(K_3\Delta p^* + K_4\Delta p^{*2}\right) \quad \text{(G3)}$$

Table 1 Constants for Eqs. (G1) and (G2)

j	C_1	C_2	C_3	C_4	D_1	D_2	D_3	D_4
0	1.1475	−0.1065	0.8662	−0.0798	1.1621	−0.0705	0.8141	−0.208
2	1.0694	−0.0969	0.9308	−0.0895	0.7853	−0.0466	1.2074	−0.322
3	1.0572	−0.0969	0.9426	−0.0893	0.9902	−0.0625	0.9622	−0.2518

Table 2 Constants for Eq. (G3)

j	K_1	K_2	K_3	K_4
0	1.1785	−0.2038	0.1093	0.1674
2	0.9913	−0.1662	0.0891	0.1447
3	1.0041	−0.1667	0.0760	0.1258

where $\chi = 2\hat{\sigma}/(2 - \hat{\sigma})$ and the constants of Eqs. (G1) and (G2) are listed in Table 1 and the constants of Eq. (G3) are listed in Table 2. We have provided constants fit to our data for $j = 0, 2, 3$ for higher accuracy. As discussed in Sec. 3.5, flux varies little with internal degrees-of-freedom; however, T_K^* is more sensitive to j and the appropriate constants should be used for Eq. (G3).

Our data falls within 5.5% of Eq. (G1) and 8% of Eq. (G2) for $-0.5 \leq \Delta p^* \leq 0.5$ for all values of j, or within 3% and 5%, respectively, at lower fluxes ($-0.25 \leq \Delta p^* \leq 0.25$). The fitting data for condensation uses $T_K = 1$ for $j = 0, 2$ and $T_K = T_{\text{sat}}(p_K)$ of water at $T_L = 25\,^\circ\text{C}$ for $j = 3$. We fit Eq. (G3) to evaporation data only, and it deviates by less than 0.5% from our data for all values of j. For condensation, we recommend modeling the temperature ratio with Eq. (17) because Eq. (G3) does not provide accurate trends for net condensation. The temperature ratios predicted by Eq. (17) fall within 4% of the Holway calculated $T_{K,\text{Holway}}^*\left(\Delta p^*, J_{\text{Eq. (G2)}}^*(\Delta p^*)\right)$ for all values of j over the range $-0.5 \leq \Delta p^* < 0$. At lower fluxes ($-0.25 \leq \Delta p^* < 0$), Eq. (17) deviates by less than 0.5%, 1.5%, and 3% for $j = 0, 2$, and 3, respectively. Note that $T_{K,\text{Eq.(17)}}^*(\Delta p^*)$ is closer to $T_{K,\text{Holway}}^*(\Delta p^*, J_{\text{Eq. (G2)}}^*(\Delta p^*))$ than $T_{K,\text{Holway}}^*(\Delta p^*, J_{\text{Eq. (16)}}^*(\Delta p^*))$; the comparison to the latter is shown in Fig. 9.

References

[1] Schrage, R. W., 1954, *A Theoretical Study of Interphase Mass Transfer*, Columbia Press, New York.

[2] Hertz, H., 1882, "Ueber Die Verdunstung Der Flüssigkeiten, Insbesondere Des Quecksilbers, Im Luftleeren Raume," Ann. Phys. Chem., **253**(10), pp. 177–200.

[3] Knudsen, M., 1915, "Die Maximale Verdampfunggeschwindigkeit Des Quecksilbers," Ann. Phys. Chem., **352**(13), pp. 697–708.

[4] Kucherov, R. Y., and Rikenglaski, L. E., 1960, "On Hydrodynamic Boundary Conditions With Evaporation of a Solid Absorbing Radiant Energy," Sov. Phys. JETP, **37**, pp. 10–11.

[5] Barrett, J., and Clement, C., 1992, "Kinetic Evaporation and Condensation Rates and Their Coefficients," J. Colloid Interface Sci., **150**(2), pp. 352–364.

[6] Anisimov, S. I., 1968, "Metal Evaporation by Laser Radiation," J. Eksperim. Teor. Fis., **54**, pp. 339–342.

[7] Ytrehus, T., 1977, "Theory and Experiments on Gas Kinetics in Evaporation," *Rarefied Gas Dynamics*, American Institute of Aeronautics and Astronautics, New York, pp. 1197–1212.

[8] Pao, Y., 1971, "Application of Kinetic Theory to the Problem of Evaporation and Condensation," Phys. Fluids, **14**(2), p. 306.

[9] Sone, Y., and Onishi, Y., 1978, "Kinetic Theory of Evaporation and Condensation –Hydrodynamic Equation and Slip Boundary Condition," J. Phys. Soc. Jpn., **44**(6), pp. 1981–1994.

[10] Cercignani, C., Fiszdon, W., and Frezzotti, A., 1985, "The Paradox of the Inverted Temperature Profiles Between an Evaporating and a Condensing Surface," Phys. Fluids, **28**(11), p. 3237.

[11] Yu, J., and Wang, H., 2012, "A Molecular Dynamics Investigation on Evaporation of Thin Liquid Films," Int. J. Heat Mass Transfer, **55**(4), pp. 1218–1225.

[12] Liang, Z., Biben, T., and Keblinski, P., 2017, "Molecular Simulation of Steady-State Evaporation and Condensation: Validity of the Schrage Relationships," Int. J. Heat Mass Transfer, **114**, pp. 105–114.

[13] Bird, E., Gutierrez Plascencia, J., and Liang, Z., 2020, "Thermal Transport Across the Interface Between Liquid n -Dodecane and Its Own Vapor: A Molecular Dynamics Study," J. Chem. Phys., **152**(18), p. 184701.

[14] Chandra, A., and Keblinski, P., 2020, "Investigating the Validity of Schrage Relationships for Water Using Molecular Dynamics Simulations," J. Chem. Phys., **153**(12), p. 124505.

[15] Sone, Y., 2007, *Molecular Gas Dynamics Theory, Techniques, and Applications*, Birkhauser, Boston, MA.

[16] Meland, R., and Ytrehus, T., 2003, "Evaporation and Condensation Knudsen Layers for Nonunity Condensation Coefficient," Phys. Fluids, **15**(5), pp. 1348–1350.

[17] Meland, R., 2003, "Molecular Dynamics Simulation of the Inverted Temperature Gradient Phenomenon," Phys. Fluids, **15**(10), p. 3244.

[18] Aoki, K., and Cercignani, C., 1983, "Evaporation and Condensation on Two Parallel Plates at Finite Reynolds Numbers," Phys. Fluids, **26**(5), p. 1163.

[19] Plesset, M. S., 1952, "Note on the Flow of Vapor Between Liquid Surfaces," J. Chem. Phys., **20**(5), pp. 790–793.

[20] Shankar, P. N., and Deshpande, M. D., 1991, "The Gas Dynamics of Massive Evaporation and Condensation," Philos. Trans. R. Soc. London. Ser. A Phys. Eng. Sci., **335**(1639), pp. 487–511.

[21] Ytrehus, T., 1997, "Molecular-Flow Effects in Evaporation and Condensation Phenomena," Multiphase Sci. Technol., **9**(3), pp. 205–327.

[22] Graur, I. A., Gatapova, E. Y., Wolf, M., and Batueva, M. A., 2021, "Non-Equilibrium Evaporation: 1D Benchmark Problem for Single Gas," Int. J. Heat Mass Transfer, **181**, p. 121997.

[23] Nabavian, K., and Bromley, L. A., 1963, "Condensation Coefficient of Water," Chem. Eng. Sci., **18**(10), pp. 651–660.

[24] Carey, V. P., 1992, *Liquid Vapor Phase Change Phenomena: An Introduction to the Thermophysics of Vaporization and Condensation Processes in Heat Transfer Equipment*, Hemisphere Publishing, Boca Raton, FL.

[25] Zhakhovskii, V. V., and Anisimov, S. I., 1997, "Molecular-Dynamics Simulation of Evaporation of a Liquid," J. Exp. Theor. Phys., **84**(4), pp. 734–745.

[26] Ishiyama, T., Yano, T., and Fujikawa, S., 2004, "Molecular Dynamics Study of Kinetic Boundary Condition at an Interface Between Argon Vapor and Its Condensed Phase," Phys. Fluids, **16**(8), pp. 2899–2906.

[27] Ishiyama, T., Yano, T., and Fujikawa, S., 2004, "Molecular Dynamics Study of Kinetic Boundary Condition at an Interface Between a Polyatomic Vapor and Its Condensed Phase," Phys. Fluids, **16**(12), pp. 4713–4726.

[28] Frezzotti, A., and Barbante, P., 2017, "Kinetic Theory Aspects of Non-Equilibrium Liquid-Vapor Flows," Mech. Eng. Rev., **4**(2), p. 16.

[29] Tsuruta, T., Tanaka, H., and Masuoka, T., 1999, "Condensation/Evaporation Coefficient and Velocity Distributions at Liquid-Vapor Interface," Int. J. Heat Mass Transfer, **42**(22), pp. 4107–4116.

[30] Kobayashi, K., Hori, K., Kon, M., Sasaki, K., and Watanabe, M., 2016, "Molecular Dynamics Study on Evaporation and Reflection of Monatomic Molecules to Construct Kinetic Boundary Condition in Vapor–Liquid Equilibria," Heat Mass Transfer, **52**(9), pp. 1851–1859.

[31] Skarbalius, G., Džiugys, A., Misiulis, E., and Navakas, R., 2021, "Molecular Dynamics Study on Water Evaporation/Condensation Parameters," Microfluid. Nanofluid., **25**(10), p. 81.

[32] Wilhelmsen, Ø., Trinh, T. T., Lervik, A., Badam, V. K., Kjelstrup, S., and Bedeaux, D., 2016, "Coherent Description of Transport Across the Water Interface: From Nanodroplets to Climate Models," Phys. Rev. E, **93**(3), p. 032801.

[33] Eames, I. W., Marr, N. J., and Sabir, H., 1997, "The Evaporation Coefficient of Water: A Review," Int. J. Heat Mass Transfer, **40**(12), pp. 2963–2973.

[34] Marek, R., and Straub, J., 2001, "Analysis of the Evaporation Coefficient and the Condensation Coefficient of Water," Int. J. Heat Mass Transfer, **44**(1), pp. 39–53.

[35] PAUL, B., 1962, "Compilation of Evaporation Coefficients," ARS J., **32**(9), pp. 1321–1328.

[36] Vaartstra, G., Zhang, L., Lu, Z., Díaz-Marín, C. D., Grossman, J. C., and Wang, E. N., 2020, "Capillary-Fed, Thin Film Evaporation Devices," J. Appl. Phys., **128**(13), p. 130901.

[37] Vincenti, W. G., and Kruger, C. H., 1965, *Introduction to Physical Gas Dynamics*, Wiley, New York.

[38] Cercignani, C., 2000, *Rarefied Gas Dynamics: From Basic Concepts to Actual Calculations*, Cambridge University Press, Cambridge, UK.

[39] Umur, A., and Griffith, P., 1965, "Mechanism of Dropwise Condensation," ASME J. Heat Transfer-Trans. ASME, **87**(2), pp. 275–282.

[40] Faghri, A., 1995, *Heat Pipe Science and Technology*, Taylor & Francis, Washington, DC.

[41] Wang, H., Garimella, S. V., and Murthy, J. Y., 2008, "An Analytical Solution for the Total Heat Transfer in the Thin-Film Region of an Evaporating Meniscus," Int. J. Heat Mass Transfer, **51**(25–26), pp. 6317–6322.

[42] Sone, Y., 2000, "Kinetic Theoretical Studies of the Half-Space Problem of Evaporation and Condensation," Transp. Theory Stat. Phys., **29**(3–5), pp. 227–260.

[43] Frezzotti, A., 2007, "A Numerical Investigation of the Steady Evaporation of a Polyatomic Gas," Eur. J. Mech. B/Fluids, **26**(1), pp. 93–104.

[44] Siewert, C. E., and Thomas, J. R., 1973, "Half-Space Problems in the Kinetic Theory of Gases," Phys. Fluids, **16**(9), p. 1557.

[45] Sone, Y., Ohwada, T., and Aoki, K., 1989, "Evaporation and Condensation on a Plane Condensed Phase: Numerical Analysis of the Linearized Boltzmann Equation for Hard-Sphere Molecules," Phys. Fluids A Fluid Dyn., **1**(8), pp. 1398–1405.

[46] Luikov, A. V., Perelman, T. L., and Anisimov, S. I., 1971, "Evaporation of a Solid Into Vacuum," Int. J. Heat Mass Transfer, **14**(2), pp. 177–184.

[47] Ytrehus, T., and Alvestad, J. A., 1981, "A Mott-Smith Solution for Nonlinear Condensation," *Rarefied Gas Dynamics, Part I*, American Institute of Aeronautics and Astronautics, New York, pp. 330–345.

[48] Shankar, P. N., and Marble, F. E., 1971, "Kinetic Theory of Transient Condensation and Evaporation at a Plane Surface," Phys. Fluids, **14**(3), p. 510.

[49] Bhatnagar, P. L., Gross, E. P., and Krook, M., 1954, "A Model for Collision Processes in Gases. I. Small Amplitude Processes in Charged and Neutral One-Component Systems," Phys. Rev., **94**(3), pp. 511–525.

[50] Welander, P., 1954, "On the Temperature Jump in a Rarefied Gas," Ark. Fys., **7**, pp. 507–553.

[51] Aoki, K., Sone, Y., and Yamada, T., 1990, "Numerical Analysis of Gas Flows Condensing on Its Plane Condensed Phase on the Basis of Kinetic Theory," Phys. Fluids A Fluid Dyn., **2**(10), pp. 1867–1878.

[52] Kogan, M. N., and Makashev, N. K., 1974, "Role of the Knudsen Layer in the Theory of Heterogeneous Reactions and in Flows With Surface Reactions," Fluid Dyn., **6**(6), pp. 913–920.

[53] Bird, G. A., 1976, *Molecular Gas Dynamics*, Clarendon Press, Oxford, UK.

[54] Bird, G. A., 1994, *Molecular Gas Dynamics and the Direct Simulation of Gas Flows*, Oxford University Press, New York.

[55] Frezzotti, A., and Ytrehus, T., 2006, "Kinetic Theory Study of Steady Condensation of a Polyatomic Gas," Phys. Fluids, **18**(2), p. 027101.

[56] Borgnakke, C., and Larsen, P. S., 1975, "Statistical Collision Model for Monte Carlo Simulation of Polyatomic Gas Mixture," J. Comput. Phys., **18**(4), pp. 405–420.

[57] Holway, L. H., 1966, "New Statistical Models for Kinetic Theory: Methods of Construction," Phys. Fluids, **9**(9), p. 1658.

[58] Lu, Z., Kinefuchi, I., Wilke, K. L., Vaartstra, G., and Wang, E. N., 2019, "A Unified Relationship for Evaporation Kinetics at Low Mach Numbers," Nat. Commun., **10**(1), p. 2368.

[59] Ginoux, J. J., 1978, *Two-Phase Flows and Heat Transfer With Application to Nuclear Reactor Design Problems*, Hemisphere Publishing Corporation, Washington, DC.

[60] Stultz, S. C., and Kitto, J. B., eds., 1992, *Steam/Its Generation and Use*, The Babcock & Wilcox, Barberton, OH.

[61] Spiegler, K. S., and El-Sayed, Y. M., 1994, *A Desalination Primer*, Balaban Desalination Publishers, Santa Maria Imbaro, Italy.

[62] Davis, E. J., 2006, "A History and State-of-the-Art of Accommodation Coefficients," Atmos. Res., **82**(3–4), pp. 561–578.

[63] Tamir, A., and Hasson, D., 1971, "Evaporation and Condensation Coefficient of Water," Chem. Eng. J., **2**(3), pp. 200–211.

[64] Smith, J. D., Cappa, C. D., Drisdell, W. S., Cohen, R. C., and Saykally, R. J., 2006, "Raman Thermometry Measurements of Free Evaporation From Liquid Water Droplets," J. Am. Chem. Soc., **128**(39), pp. 12892–12898.

[65] Li, Y., Chen, H., Xiao, S., Alibakhshi, M. A., Lo, C.-W., Lu, M.-C., and Duan, C., 2019, "Ultrafast Diameter-Dependent Water Evaporation From Nanopores," ACS Nano, **13**(3), pp. 3363–3372.

[66] Meland, R., Frezzotti, A., Ytrehus, T., and Hafskjold, B., 2004, "Nonequilibrium Molecular-Dynamics Simulation of Net Evaporation and Net Condensation, and Evaluation of the Gas-Kinetic Boundary Condition at the Interphase," Phys. Fluids, **16**(2), pp. 223–243.

[67] Mott-Smith, H. M., 1951, "The Solution of the Boltzmann Equation for a Shock Wave," Phys. Rev., **82**(6), pp. 885–892.

[68] Cercignani, C., 1980, "Strong Evaporation of a Polyatomic Gas," Rarefied Gas Dynamics; International Symposium, 12th, Charlottesville, VA, July 7–11, Technical Papers. Part 1, American Institute of Aeronautics and Astronautics, New York, pp. 305–320.

[69] Kogan, M. N., 1992, "Kinetic Theory in Aerothermodynamics," Prog. Aerosp. Sci., **29**(4), pp. 271–354.

[70] Abramov, A. A., and Kogan, M. N., 1984, "Conditions for Supersonic Condensation of Gas," Dokl. Akad. Nauk SSSR, **278**(5), pp. 1078–1081.

[71] Aoki, K., Nishino, K., Sone, Y., and Sugimoto, H., 1991, "Numerical Analysis of Steady Flows of a Gas Condensing on or Evaporating From Its Plane Condensed Phase on the Basis of Kinetic Theory: Effect of Gas Motion Along the Condensed Phase," Phys. Fluids A Fluid Dyn., **3**(9), pp. 2260–2275.

[72] Chu, C. K., 1965, "Kinetic-Theoretic Description of the Formation of a Shock Wave," Phys. Fluids, **8**(1), p. 12.

[73] Ytrehus, T., 1983, "Asymmetries in Evaporation and Condensation Knudsen Layer Problems," Phys. Fluids, **26**(4), p. 939.